arXiv:astro-ph/0207249v1 11 Jul 2002

AGN Black Hole Masses and Bolometric Luminosities

Jong-Hak Woo

Department of Astronomy, Yale University, P.O. Box 208101, New Haven, CT 06520-8101

jhwoo@astro.yale.edu

C. Megan Urry

Department of Physics and Center for Astronomy and Astrophysics, Yale University, P.O. Box 208121, New Haven, CT 06520-8121

meg.urry@yale.edu

ABSTRACT

Black hole mass, along with mass accretion rate, is a fundamental property of active galactic nuclei. Black hole mass sets an approximate upper limit to AGN energetics via the Eddington limit. We collect and compare all AGN black hole mass estimates from the literature; these 177 masses are mostly based on the virial assumption for the broad emission lines, with the broad-line region size determined from either reverberation mapping or optical luminosity. We introduce 200 additional black hole mass estimates based on properties of the host galaxy bulges, using either the observed stellar velocity dispersion or using the fundamental plane relation to infer σ; these methods assume that AGN hosts are normal galaxies. We compare 36 cases for which black hole mass has been generated by different methods and find, for individual objects, a scatter as high as a couple of orders of magnitude. The less direct the method, the larger the discrepancy with other estimates, probably due to the large scatter in the underlying correlations assumed. Using published fluxes, we calculate bolometric luminosities for 234 AGNs and investigate the relation between black hole mass and luminosity. In contrast to other studies, we find no significant correlation of black hole mass with luminosity, other than those induced by circular reasoning in the estimation of black hole mass. The Eddington limit defines an approximate upper envelope to the distribution of luminosities, but the lower envelope depends entirely on the sample of AGN included. For any given black hole mass, there is a range in Eddington ratio of up to three orders of magnitude.

Subject headings: galaxies: active - quasars: general - mass–luminosity relation

1. Introduction

Black holes have been the leading candidate to power the central engines in AGN for over three decades (Lynden-Bell 1969), but direct evidence for their presence has been elusive. In nearby galaxies, spatially resolved kinematics have provided strong evidence for the ubiquity of nuclear black holes, with dynamical black hole detections reported for 37 galaxies (Kormendy & Gebhardt 2001). Such observations are available only for a handful of the nearest AGN (Harms et al. 1994, Miyoshi et al. 1995, Greenhill et al. 1996).

Black hole mass, along with mass accretion rate, is a fundamental property of AGN. Via the Eddington limit, a maximum luminosity for the idealized case of spherical accretion ($L_{Edd} = 1.25 \times 10^{38} \times M_{BH}/M_{\odot}$ ergs s^{-1}), the black hole mass sets an approximate upper limit to AGN energetics. It is also the integral of the accretion history of the AGN. However, direct kinematic observations of the black hole mass are limited by finite spatial resolution (a typical AGN at redshift 2 would require nano-arcsecond resolution to probe the sphere of influence of the black hole), not to mention that scattered light from the bright central source dilutes any kinematic signal from orbiting material.

For these reasons, various less direct methods for estimating black hole mass have been devised. One set of methods (§§ 2.1,2.2) assumes the broad-line region (BLR) is gravitationally bound by the central black hole potential, so that the black hole mass can be estimated from the orbital radius and the Doppler velocity. The reverberation mapping technique utilizes the time lag between continum and emission lines to derive the distance of the BLR from the black hole (Blandford & McKee 1982, Peterson 1993). About three dozen AGN black hole masses have been measured using this technique. A less costly alternative is to infer the BLR size from the optical or ultraviolet luminosity (McLure & Dunlop 2001, Vestergaard 2002), with which it is correlated, at least over a limited range of luminosities (Kaspi et al. 2000).

A different approach to estimating black hole mass is to exploit the correlation, seen in nearby normal galaxies, between black hole mass and stellar velocity dispersion, σ (Ferrarese & Merritt 2000, Gebhardt et al. 2000a). If AGN host galaxies are similar to non-active galaxies, this correlation should hold also for them. Since stellar velocity dispersion measurements are still difficult for higher redshift AGN, the stellar velocity dispersion can possibly be inferred from effective radius and central surface brightness assuming AGN host galaxies occupy the same fundamental plane as ordinary ellipticals (O'Dowd et al. 2002).

Some previous studies have found a tight relation between mass and luminosity in AGN (Dibai 1981, Wandel & Yahil 1985, Padovani & Rafanelli 1988, Koratkar & Gaskell 1991, Kaspi et al. 2000); however, the scatter is large when the black hole masses are restricted

to the most reliable estimates (from reverberation mapping). One might have expected a correlation between AGN black hole mass and luminosity since the Eddington luminosity is proportional to black hole mass, but if there is a range in accretion rates and/or efficiencies, the relation will be weaker.

In this paper, we collect and compare all AGN black hole mass estimates from the literature, and we make new black hole mass estimates from stellar velocity dispersions (§ 2). We calculate bolometric luminosities for these same AGN to investigate their mass–luminosity relation, and look for trends of Eddington ratio with luminosity (§ 3). Table 1 summarizes the number of black hole mass estimates from the various methods. We use $H_0 = 75$ km s^{-1} and $q_0 = 0.5$ throughout this paper.

2. Black Hole Masses in AGN

Very few black hole masses in AGN have been measured with spatially resolved dynamics near the central black hole which is the preferred method for estimating black hole mass in nearby (inactive) galaxies. The two cases in which this has been done with maser kinematics (NGC 1068 and NGC 4258) are listed in Table 2. Remaining black hole masses are determined with less direct methods.

2.1. Masses from the Virialized Motion

Assuming that broad-line clouds are virialized, for which there has been increasing evidence (Krolik et al. 1991, Wandel et al. 1999, cf. Krolik 2001), the black hole mass can be estimated:

$$M_{BH} = R_{BLR}\ v^2\ G^{-1}\ . \tag{1}$$

The virial assumption may not be correct, however; radiation pressure and/or magnetic fields may contribute significantly to the dynamics (Krolik 2001), and outflows or winds could cause the observed line widths to exceed those induced by the black hole potential alone. In these cases the black hole mass calculated from Eq. 1 would be overestimated.

2.1.1. Reverberation Mapping Estimates

In reverberation mapping, the BLR size is estimated from the time lag between the ionizing continuum and the broad-line strength (Peterson 1993). To date, 36 AGN black hole

masses have been measured from combining reverberation-mapped BLR sizes with broad-line velocities (Wandel et al. 1999, Ho 1999, Kaspi et al. 2000, Onken & Peterson 2002). These are listed in Table 3, along with the redshifts, bolometric luminosities, and published AGN types.

Contributing to the uncertainty in the black hole mass estimation are the BLR orbits and velocities assumed. The broad line velocity can be determined from the observed spectra, either as the mean of the FWHM derived from each line or as the FWHM from the root mean square (rms) spectrum (Peterson et al. 1988). Kaspi et al. (2000) showed that the two velocity estimates are similar; however, the difference between the two gives black hole mass uncertainties as large as a factor of ten (Figure 1).

Assumptions about the orbital shape and inclination of the broad-line clouds introduce additional uncertainties. An isotropic distribution with random inclinations is often assumed for the broad-line clouds, in which case velocity is derived from Equation (2) with $f = \sqrt{3}/2$ (Netzer 1990):

$$v = f \times FWHM \ . \tag{2}$$

However, the random orbits assumption may not be valid for quasars. McLure & Dunlop (2001) reproduced the FHWM distribution of Seyferts and quasars with two disc components, and determined that the average relationship between observed FWHM and actual orbital velocity corresponds to $f = 3/2$. Thus for the same AGN, the black hole mass estimates in McLure & Dunlop (2001) are factor of 3 larger than those of Kaspi et al. (2000). Considering orbital shape alone, the full range of uncertainty in mass appears to be 2 orders of magnitude, from $f = 3/2$ to ~ 200 (Krolik 2001).

In Figure 1 we compare 34 reverberation-mapped black hole masses calculated for two different estimates of the broad-line velocities (Kaspi et al. 2000). The derived black hole masses for a given object differ by less than an order of magnitude, making reverberation mapping one of the more robust techniques for estimating AGN black hole masses. It is however resource intensive, time consuming, and not applicable to most AGN (those without broad lines). Consequently, relatively few AGN black hole masses have been well estimated.

2.1.2. Black Hole Mass Estimates using the BLR Size – Luminosity Relation

Since reverberation mapping is a laborious process, alternative ways of deriving the BLR size are of interest. Several authors have noted that R_{BLR} (where known from reverberation

mapping) appears to correlate with UV/optical luminosity (Koratkar & Gaskell 1991, Kaspi et al. 1996, Wandel et al. 1999, Kaspi et al. 2000). The proportionality has been reported as $L_{opt}^{1/2}$ (Wandel et al. 1999), which corresponds to a constant ionization parameter, but in the most recent studies appears to be $R_{BLR} \propto L^{0.7}_{5100\mathrm{A}^\circ}$ (Kaspi et al. 2000, Vestergaard et al. 2002; cf. McLure & Jarvis 2002). Using this relation and assuming random isotropic orbits ($f = \sqrt{3}/2$ in Eq. 2), we obtain:

$$M_{BH} = 4.817 \times (\frac{\lambda L_\lambda(5100\mathrm{\AA})}{10^{44}\ \mathrm{ergss}^{-1}})^{0.7} \times\ (FHWM)^2\ . \tag{3}$$

There is large scatter in the $R_{BLR} - L_{5100\mathrm{A}^\circ}$ correlation (e.g., Figure 7 of Kaspi et al. 2000), and it has been established only over a limited range of luminosities, hence it yields correspondingly uncertain black hole masses. We list these values in Table 4, along with the redshift, bolometric luminosity, and AGN type, and in Figure 2 we compare them to all available reverberation mapping estimates. The differences range up to an order of magnitude, with an rms difference of 0.50 in the log of the ratio.

If optical luminosity is well correlated with bolometric luminosity, the fitted correlation of Kaspi et al. (2000) leads to a precise relation between black hole mass and bolometric luminosity (something we would like to investigate rather than assume). The Eddington ratio (i.e., the ratio of bolometric luminosity to Eddington luminosity) would then depend on bolometric luminosity to the 0.3 power.

Although there are some concerns, black hole mass estimates with this method remain important given the difficulty of more accurate estimates and the relatively small number of AGN for which any black hole mass estimates have been made. Thus, we collected all such black hole mass estimates available in the literature (26 from McLure & Dunlop 2001, 3 from Laor 2001, 80 from Gu et al. 2001, 30 from Oshlack, Webster & Whiting 2002), re-computed using Eq. 3 for consistency with our cosmology.

2.2. Black Hole Mass from Stellar Velocity Dispersion

In nearby galaxies there is apparently a close connection between the central black hole and the bulge kinematics. Specifically, black hole mass (determined from spatially resolved kinematics) correlates well with stellar velocity dispersion, as $M_{BH} \propto \sigma^{3.75}$ (Gebhardt et al. 2000a) or $M_{BH} \propto \sigma^{4.8}$ (Ferrarese & Merritt 2000). From the collective analysis by Tremaine et al. (2002):

$$M_{BH} = 1.349 \times 10^8 M_\odot (\sigma/200\mathrm{km\ s}^{-1})^{4.02}\ . \tag{4}$$

AGN host galaxies appear to be very much like normal galaxies. This is particularly well established for radio-loud AGN, whose host galaxies follow the usual Kormendy relation (Taylor et al. 1996; McLure et al. 1999; Urry et al. 2000; Bettoni et al. 2001). Present data on host galaxies are in accord with the "grand unification" hypothesis, suggested on other grounds, that AGN are simply a transient phase of normal galaxies (Cavaliere & Padovani 1989). Therefore it is reasonable to expect that the same M_{BH}–σ correlation should be present in AGN host galaxies, in which case we can use Eq. 4 to infer black hole mass. Gebhardt et al. (2000b) and Ferrarese et al. (2001) estimated black hole masses in this way for a few Seyfert galaxies (7 and 6 respectively), and found good agreement with reverberation mapping values.

2.2.1. From Direct Measurement of Stellar Velocity Dispersion

An increasing number of AGN have published measurements of stellar velocity dispersion. Black hole masses calculated from σ have been published for 21 Seyferts (Wu & Han 2001) and 12 BL Lac objects (Falomo et al. 2002; Barth, Ho & Sargent 2002); we rescaled these to our cosmology as needed. From the literature we collected velocity dispersions for an additional 108 AGN (36 Seyfert galaxies and 72 radio galaxies), and calculated their black hole masses according to Eq. 4. All 141 black hole masses are presented in Table 5.

For 14 Seyfert galaxies both velocity dispersions and reverberation-mapped BLR sizes are available. In Figure 3 we compare the two associated black hole mass estimates. They agree relatively well, with scatter much less than an order of magnitude.

2.2.2. From Indirect Estimates of Stellar Velocity Dispersion

Stellar velocity dispersions are not extensively known for AGN host galaxies, nor are they easy to measure, particularly at higher redshift. However, by the same "grand unification" of host galaxies with normal galaxies, we can infer the velocity dispersions (albeit with additional scatter) from the morphological parameters of the bulge: r_e, the effective radius, and μ_e, the surface brightness at that radius. These have been very well measured for more than 100 AGN using the excellent spatial resolution of the Hubble Space Telescope[1] (HST),

[1]Based on observations made with the NASA/ESA Hubble Space Telescope, obtained at the Space Telescope Science Institute, which is operated by the Association of Universities for Research in Astronomy, Inc., under NASA contract NAS 5-26555. These observations are associated with proposals # 5849, 5938, 5939, 5949, 5957, 5974, 5982, 5988, 6303, 6361, 6363, 6490, 6776, 7893.

which yields more robust results than observations in typical ground-based seeing.

Thus, at least for radio-loud AGN, black hole mass can be derived from r_e and μ_e (O'Dowd et al. 2002). If sufficiently accurate, this would be an extremely valuable method since the required imaging data are much easier to obtain than σ, and such a method could be applied widely and at higher redshift than the direct method.

Using this method, we estimate 59 new black hole masses for 45 BL Lac objects, 10 radio galaxies, and 4 radio-quiet AGN, all of which have host galaxies detected with HST. Surface brightnesses and effective radii from Urry et al. (2000) and Dunlop et al. (2002) are used to derive stellar velocity dispersion via fundamental plane relation of Jorgensen et al. (1996):

$$\log r_e = 1.24\ log\sigma - 0.82\ log < I_e > +0.2132\ z - 0.00131 - C\ . \tag{5}$$

Here, $C = 0.176$ for cosmological correction to H_0=75 km s^{-1}. Black hole masses are then estimated using Eq. 4. Morphological parameters and derived black hole masses are given in Table 6. Bolometric luminosity is not straightforward to derive for most of these objects because of beaming and obscuration.

To test the accuracy of this fundamental plane method for estimating black hole mass, we considered 72 radio galaxies for which all three parameters of the fundamental plane are measured (Bettoni et al. 2001).[2] Figure 4 shows the comparison of black hole masses derived indirectly from μ_e and r_e with those derived directly from σ. (This is in effect an unusual projection of the fundamental plane.) Points are coded to highlight the homogeneous data of Bettoni et al. (filled circles), which are more tightly correlated than the additional heterogeneous data (open squares and crosses) collected by them. The six most extreme outliers are marked with crosses. The mean black hole masses determined by the two methods agree to within 10%, while the rms scatter is a factor of 4 or so (slightly higher for the heterogeneous data than for the homogeneous data).

Although the fundamental plane method introduces additional scatter compared to direct measurement of stellar velocity dispersion, estimating black hole masses in this way is so far one of the few ways to infer AGN black hole mass for high redshift AGN (perhaps the only method for AGN that lack broad emission lines). Of course, the underlying assumption of "grand unification" of AGN and galaxies remains untested, particularly at high redshift.

[2]Table 3 of Bettoni et al. (2001) apparently lists r_e values in arcsec rather than kpc (Barth et al. 2002).

3. Bolometric Luminosity and Black Hole Mass

3.1. Bolometric Luminosity of AGN

Bolometric luminosity of AGN is sometimes approximated from optical luminosity, since integration of the spectral energy distribution (SED), which spans many decades in wavelength, is usually hampered by lack of wavelength coverage and by variability. Here we are able in many cases to determine bolometric luminosity by integrating all available flux points in the SED. This is particularly important given the role of optical luminosity in deriving some black hole masses, otherwise correlations between M_{BH} and L_{bol} can be induced.

For 234 of the 377 AGN for which black hole mass has been estimated in the Tables, we were able to determine bolometric luminosity. The other 143 objects are radio galaxies and BL Lac objects, for which obscuration and beaming are significant. For 82 of the 234, there are numerous published fluxes from ultraviolet to far-infrared wavelengths, which we collected using the NED database.[3] Multiple observations for the same band were simply averaged, and the Galactic extinction law (Cardelli, Clayton & Mathis 1989) was used to correct for dust (with A_V also taken from NED). We then integrated these SEDs directly to get the bolometric luminosity.

For the remaining AGN, mostly quasars at relatively high redshift, sufficient flux points were unavailable. In 152 cases, including most of the luminous quasars, we obtained the bolometric luminosity by fitting the average SED for that AGN type to the available flux points. Average SEDs are from various sources: radio-loud and radio-quiet quasar SEDs are from Elvis et al. (1994); Seyfert 1 SEDs are from Mas-Hesse et al. (1994); and Seyfert 2 SEDs are from Schmitt et al. (1997). Optical flux was corrected for Galactic extinction using individual reddening values from NED. We note that the bolometric luminosities are roughly 10 times the optical luminosity (precisely, in the case of SED fitting for quasars, and within a factor of 5-6 in the case of direct integration of the SEDs).

Bolometric luminosities for a total of 234 AGN are given in Tables 2, 3, 4 and 5. The associated black hole masses were estimated as follows: 2 from maser kinematics, 36 from broad-line widths plus reverberation mapping, 139 from broad-line widths plus the $L_{5100\mathrm{\AA}}$ - R_{BLR} relation, and 57 from the M_{BH} - σ relation.

In order to check our bolometric luminosity measurements, we compare them with previous estimates by Padovani & Rafanelli (1988), who integrated available optical to far-

[3]The NASA/IPAC Extragalactic Database (NED) is operated by the Jet Propulsion Laboratory, California Institute of Technology, under contract with the National Aeronautics and Space Administration.

infrared fluxes for 58 Seyfert galaxies and quasars. Twenty-six AGN in the Padovani & Rafanelli sample have bolometric luminosities estimated here; we rescaled the former values to $H_0 = 75\,\mathrm{km\,s^{-1}}$ simply by multiplying by 4/9 ($H_0 = 50\,\mathrm{km\,s^{-1}}$, $q_0 = 0$ in their calculation). The comparison is shown in Figure 5. The two estimations agree well although the Padovani & Rafanelli values may be systematically lower due to the more limited spectral range in their calculation.

3.2. The Black Hole Mass – Luminosity Relation

We now compare bolometric luminosity with black hole mass. Figure 6a includes only the 36 reverberation-mapped quasars and Seyfert galaxies, and Figure 6b includes the 57 Seyfert galaxies for which black hole mass was estimated from observed stellar velocity dispersion. There is large scatter and little correlation between bolometric luminosity and black hole mass. For a given black hole mass, the bolometric luminosity ranges over more than two orders of magnitude. Figure 6c shows the mass–luminosity plot for AGN with black hole masses that were derived from optical luminosity and broad-line velocity (McLure & Dunlop 2001, Laor 2001, Gu et al. 2001, Oshlack et al. 2002). Even here there not much more of a correlation, although one will appear if optical and bolometric luminosities are well correlated. That is, since black hole masses for these AGN were derived from $L_{5100\mathrm{\AA}}$, the slope indicated by the solid line is implied if L_{bol} is proportional to $L_{5100\mathrm{\AA}}$.

Figure 7 shows the mass–luminosity relation for all 234 AGN. Even more clearly than in Figure 6, there is hardly any trend of luminosity with black hole mass. For a given AGN black hole mass, the bolometric luminosity ranges over at least two, and as much as four, orders of magnitude. The Eddington ratio must span a similarly large range. The Eddington ratio does define an approximate (but not hard) upper limit to the distribution of luminosities; that is, points are missing from the upper left region above the dotted line, in fact previously noted by McLeod, Rieke & Storrie-Lombardi (1999). The lack of points in the lower right, however, is a selection effect: this part of the diagram gets filled in simply by including lower luminosity AGN, continuously down to galaxies. Among the low-luminosity objects with large black holes are the radio galaxies and BL Lac objects for which we do not have good estimates of bolometric luminosity (cf. O'Dowd et al. 2002); the box indicates the approximate region they occupy, calculated from the observed luminosities of BL Lacs using the family of SEDs from Fossati et al. (1998) and correcting for beaming factors in the range 3-10 (Dondi & Ghisellini 1995).

AGN lore has it that the Eddington ratio is 0.1-1 for high-luminosity sources and an order of magnitude or more smaller for low-luminosity sources. Our sample of AGN spans

5 decades in bolometric luminosity so we should be very sensitive to any such trends. In Figure 8 we plot Eddington ratio versus bolometric luminosity (top panel). At most luminosities, the Eddington ratio spans two decades or so, except at the very highest luminosity. There appears to be a deficit of high luminosity objects with low Eddington ratios (i.e., with black holes in the range $10^8 < M_{\rm BH}/M_\odot < 10^{10}$). However, these include some of the radio sources for which we do not have good bolometric luminosities (see Table 6). Furthermore, if more massive black holes are rare (i.e., there is a steep mass function), they would on average be found at high redshift, yet low-luminosity radio sources at high redshift are excluded from flux-limited samples. There is also a deficiency of points in the upper left corner of the plot; these would be AGN with luminosities of $\lesssim 10^{44}$ ergs s^{-1} and black hole masses less than 10^6 $M_\odot$. (Note that low-luminosity AGN may be more difficult to detect because of dilution by host galaxy light.) Thus there is no immediate evidence of any real trend in Eddington ratio with luminosity.

We also plot Eddington ratio versus black hole mass (bottom panel). Again, there are no clear trends that cannot be explained by sample selection effects. For example, objects with luminosities below 10^{43} ergs s^{-1} are not called Seyfert galaxies or quasars and thus do not appear in this diagram. (One could add them, and they would fill in the lower left corner of the plot.) AGN with luminosities greater than 10^{47} ergs s^{-1} are rare and thus probably too distant, on average, to have black hole mass estimates. With such a heterogeneous sample, we hesitate to make any strong statements, but certainly we see only very weak trends or correlations, and those are quite plausibly induced by sample selection effects.

We can see this by plotting the Eddington ratio versus redshift (Figure 9). Again there is little if any trend. High Eddington ratio objects ($L_{bol}/L_{Edd} \gtrsim 1$) are perhaps missing at low redshift, but this can be explained as a volume effect (i.e., given the steep luminosity function of AGN, one has to survey a large volume to find a relatively rare high-luminosity AGN). More obviously, low Eddington ratio objects $L_{bol}/L_{Edd} \gtrsim 1$) are absent at high redshift, and this is partly a flux limit issue, since low-luminosity AGN fall out of samples at high redshift. Thus any trends that do appear to the eye in this plot are explained by obvious selection effects.

3.3. Black Hole Mass and Radio Luminosity

Finally, we look at radio luminosity versus black hole mass (Fig. 10, top panel) since previous reports have suggested there is a correlation between the two (McLure et al. 1999; Lacy et al. 2001), although more recent investigations have not found such a correlation (Ho 2002; Oshlack et al 2002). Again, there is little evidence of a correlation, particularly

given the missing low-luminosity sources like BL Lacs that do appear to have high black hole masses (and thus should help fill in the lower right corner of the plot). Very low-luminosity AGN ($L < 10^{23}$ W/Hz) with massive black holes may be missing, though this is hard to quantify given the missing BL Lacs and radio galaxies.

To further investigate this point, we consider radio-loudness. There have been suggestions that black hole mass is a factor in radio loudness, such that $R > 1$ ($R \equiv L_{5\ \mathrm{GHz}}/L_{5000\ \mathrm{\AA}}$) requires $M_{BH} \gtrsim 10^9\ M_\odot$ (Laor 2000). In Figure 10 we plot radio loudness versus black hole mass for the same objects (bottom panel). The radio-loud AGN have a very broad distribution of masses, so there clearly is no threshold effect. In the radio-quiet regime ($R < 1$), the distribution of masses is narrower, with no black holes masses greater than $M_{BH} \gtrsim 10^9\ M_\odot$. We note that almost all of the high-mass black holes are estimated from the optical luminosity method; that these occur in radio-loud AGN, therefore, could be explained if an appreciable fraction of the optical luminosity is beamed. If instead the absence of high-mass radio-quiet AGN is real, this would be a very significant distinction between the radio-quiet and radio-loud AGN. However, given the heterogeneous sample discussed here, the absence of evidence of these objects is not evidence of their absence, and more work will be required on this point.

4. Summary and Conclusions

We estimated and/or collected from the literature black hole masses for 377 AGN, obtained with various methods. These span a range of nearly 4 orders of magnitude, from $10^6\ M_\odot$ to $7 \times 10^9\ M_\odot$. Direct comparisons suggest that reverberation mapping and stellar velocity dispersion give reliable black hole mass estimates — within factors of a few — while using optical luminosity to infer broad-line size or using the fundamental plane to infer velocity dispersion leads to somewhat larger uncertainties. In the case of virial estimates (reverberation mapping, optical luminosity, or other), additional uncertainties enter through the unknown orbits and the possible non-virial motions of the line-emitting gas.

We estimated bolometric luminosities for most of the AGN, apart from those affected strongly by beaming or by obscuration of the nuclear emission. Comparing bolometric luminosity to black hole mass for 234 AGN, we find little or no correlation. Gaps in coverage of the L_{bol}–M_{BH} plane are due at least in part to high-mass, low-luminosity objects like the BL Lac objects and radio galaxies for which we have no good bolometric luminosity estimates.

For a given black hole mass, bolometric luminosities range over as many as four orders

of magnitude. The Eddington ratios span nearly as large a range, 2–3 orders of magnitude at most luminosities. These are much larger than any uncertainties in the estimates of either black hole mass or luminosity. There are no strong trends of Eddington ratio with luminosity, contrary to long-held preconceptions. The absence of low Eddington ratios at high redshifts (high luminosities) can be explained at least in part by selection effects in flux-limited surveys wherein highly sub-Eddington AGN disappear progressively at higher redshifts.

We also do not confirm previously reported trends of radio luminosity with black hole mass, and while our results indicate a modest dependence of radio loudness on black hole mass, selection effects may exaggerate or even produce this trend. On the whole, black hole mass seems to have remarkably little to do with the appearance of active nuclei, either their luminosities or radio power.

Of course, the present sample includes a randomly selected mix of AGN, with black hole masses estimated in different ways, by different people, from different data sets. There may be real trends dependent on other variables not taken into account here (e.g., AGN type). It is obviously of interest to apply the more robust black hole mass estimation methods — reverberation mapping and stellar velocity dispersion — to a large sample of AGN, at as high a redshift as possible, although these methods will probably not work for the typical AGN at $z \sim 2$–3. In practice, such a study would start with measurements of stellar velocity dispersions at $0.05 \lesssim z \lesssim 0.4$, which require 4- to 10-m class telescopes.

We thank Matthew O'Dowd for suggesting the fundamental plane method of estimating black hole masses and for helpful discussions. We thank Aaron Barth for his careful reading of the manuscript, and Meredith Hughes for help with the research. Support for proposals 5938, 5939, 6363, and 7893 was provided by NASA through grants from the Space Telescope Science Institute, which is operated by the Association of Universities for Research in Astronomy, Inc., under NASA contract NAS 5-26555.

REFERENCES

Barth, A., Ho, L., & Sargent, W. L. W. 2002, ApJ, submitted

Bettoni, D., Falomo, R., Fasano, G., Govoni, F., Salvo, M., & Scarpa, R. 2001, A&A, 380, 471

Blandford, R. D., & McKee, C. F. 1982, ApJ, 255, 419

Cardelli, J. A., Clayton, G. C., & Mathis, J. 1989, ApJ, 345, 245

Cavaliere, A., & Padovani, P. 1989, ApJ, 340, L5

Dibai, E. A. 1981, Soviet Astr., 24, 389

Di Nella, H., Garcia, A. M., Garnier, R., & Paturel, G. 1995, A&AS, 113, 151

Dondi, L., & Ghisellini, G. 1995, MNRAS, 273, 583

Dunlop, J. S., McLure, R. J., Kukula, M. J., Baum, S. A., O'Dea, C. P., & Hughes, D. H. 2002, MNRAS, submitted (astro-ph/0108397)

Elvis, M., et al. 1994, ApJS, 95, 1

Falomo, R., Kotilainen, J. K., & Treves, A. 2002, ApJ, 569, L35

Ferrarese, L., & Merritt, D. 2000, ApJ, 539, L9

Ferrarese, L., et al. 2001, ApJ, 555, L79

Fossati, G., Maraschi, L., Celotti, A., Comastri, A. & Ghisellini, G. 1998, MNRAS, 299, 433

Gebhardt, K., et al. 2000a, ApJ, 539, L13

Gebhardt, K., et al. 2000b, ApJ, 543, L5

Greenhill, L. J., et al. 1996, ApJ, 481, L23

Gu, M., Cao, X., & Jiang, D. R. 2001, MNRAS, 327, 1111

Harms, R. J. et al. 1994, ApJ, 435, L35

Ho, L. C. 1999, in Observational Evidence for Black Holes in the Universe, ed. S. K. Chakrabarti (Dordrecht: Kluwer), 157

Ho, L. C. 2002, ApJ, 564, 120

Jorgensen, I., Franx, M., & Kjargaard, P. 1996, MNRAS, 280, 167

Kaspi, S., Smith, P. S., Maoz, D., Netzer, H., & Jannuzi, B. T. 1996, ApJ, 471, L75

Kaspi, S., et al. 2000, ApJ, 533, 631

Koratkar, A. P., & C. M. Gaskell 1991, ApJ, 370, L61

Krolik, J. H., et al. 1991, ApJ, 371, 541

Krolik, J. H. 2001, ApJ, 551, 72

Kormendy, J., & Gebhardt, K. 2001, in The 20th Texas Symposium on Relativistic Astrophysics, ed. H. Martel & J. C. Whleer, in press (astro-ph/0105230)

Lacy, M., Laurent-Meuleisen, S. A., Ridgway, S. E., Becker, R. H., & White, R. L. 2001, ApJ, 551, L17

Laor, A. 2000, ApJ, 543, L111

Laor, A. 2001, ApJ, 553, 677

Lynden-Bell, D. 1969, Nature, 223, 690

McLeod, K. K., Rieke, G. H., & Storrie-Lombardi, L. J. 1999 ApJ, 511, L67

McLure, R. J., Kukula, M. J., Dunlop, J. S., Baum, S. A., & O'Dea, C. P. 1999, MNRAS, 308, 377

McLure, R. J., & Dunlop, J. S. 2001, MNRAS, 327, 199

McLure, R. J., & Jarvis, M. J. 2002, MNRAS, submitted (astroph 0204473)

Mas-Hesse, J. M., et al. 1995 A&A, 298, 22

Miyoshi, M., et al. 1995, Nature, 373, 127

Nelson, C. & Whittle, M. 1995, ApJS, 99, 67

Netzer, H. 1990, in Active Galactic Nuclei: 1990 Sass-Fee Lectures, ed. T. J.-L. Courvoisier & M. Mayor (Berlin: Springer), 137

Schmitt, H., et al. 1997, AJ, 114, 592

O'Dowd, M., C. M., Urry, & R. Scarpa 2001, ApJ, submitted

Oliva, E., Origlia, L., Kotilainen, J.K., Moorwood, A.F.M. 1995, A&A 301, 55

Oliva, E., Origlia, L., Maiolino, R., Moorwood, A. F. M. 1999 A&A 350, 9

Onken, C. A. & Peterson, B. A. 2002, ApJ, acce2002, ApJ, in press

Oshlack, A., Webster, R., & Whiting, M. 2002, PASP, in press

Padovani, P., & Rafanelli, P. 1988, A&A 205, 53

Peterson, B. M. 1988, PASP, 100, 18

Peterson, B. M. 1993, PASP, 105, 247

Taylor, G. L., Dunlop, J. S., Hughes, D. H., & Robson, E. I. 1996, MNRAS, 283, 930

Tremaine, S., et al. 2002, ApJ, in press (astro-ph/0203468)

Urry, C. M., et al. 2000, ApJ, 532, 816

Vestergaard, M. 2002, ApJ, 571, 733

Wandel, A., & Yahil, A. 1985, ApJ, 295, L1

Wandel, A., Peterson, B. M., & Makkan, M. A. 1999, ApJ, 526, 579

Wu, X.-B., & Han, J. L. 2001, A&A, 380, 31

This preprint was prepared with the AAS LaTeX macros v5.0.

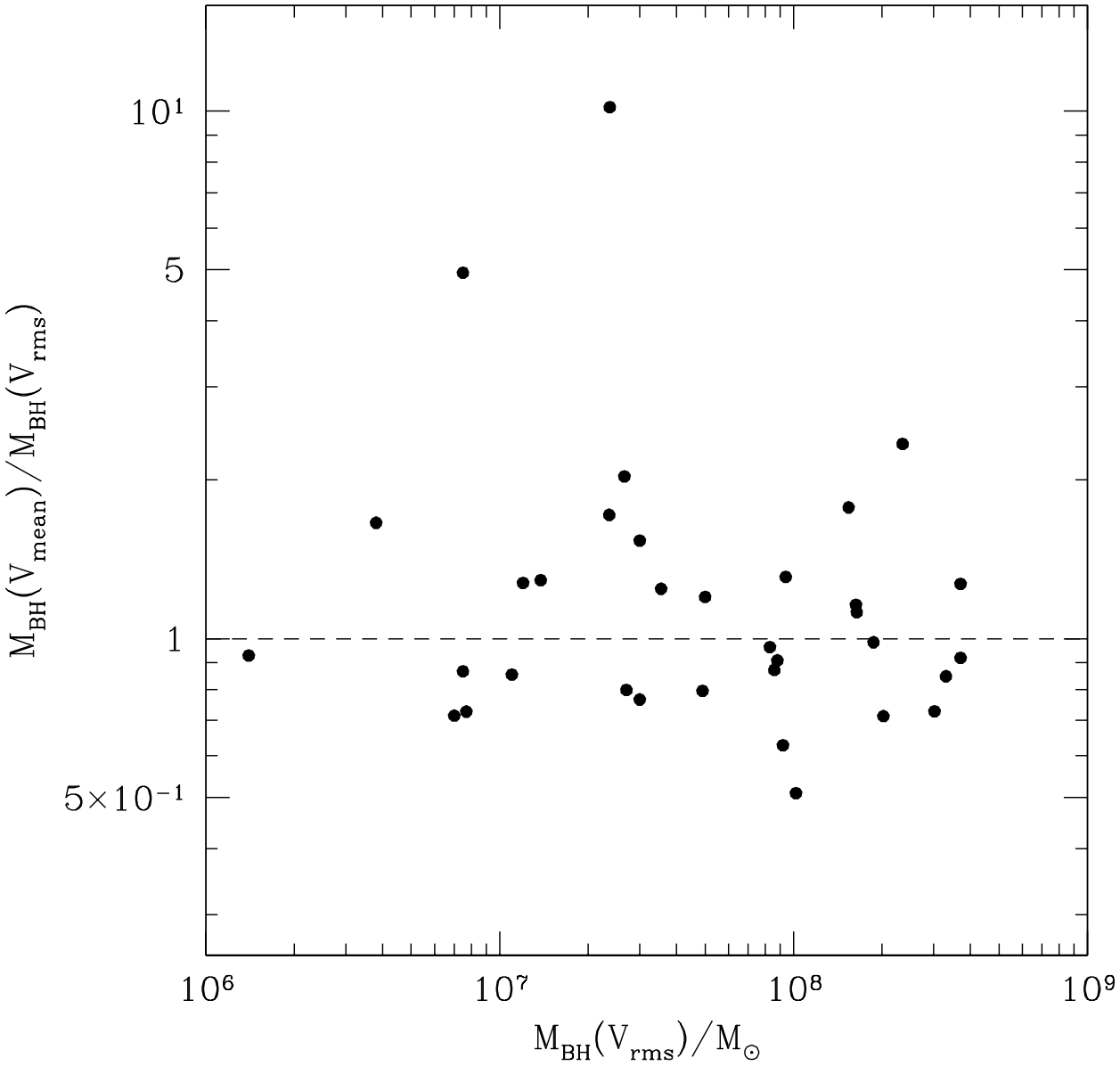

Fig. 1.— Comparison of black hole masses calculated for different FWHM estimates — mean FWHM and FWHM of the rms spectrum — for the 34 reverberation-mapped AGN of Kaspi et al. (2000). The difference in black hole mass for the same AGN is as large as an order of magnitude.

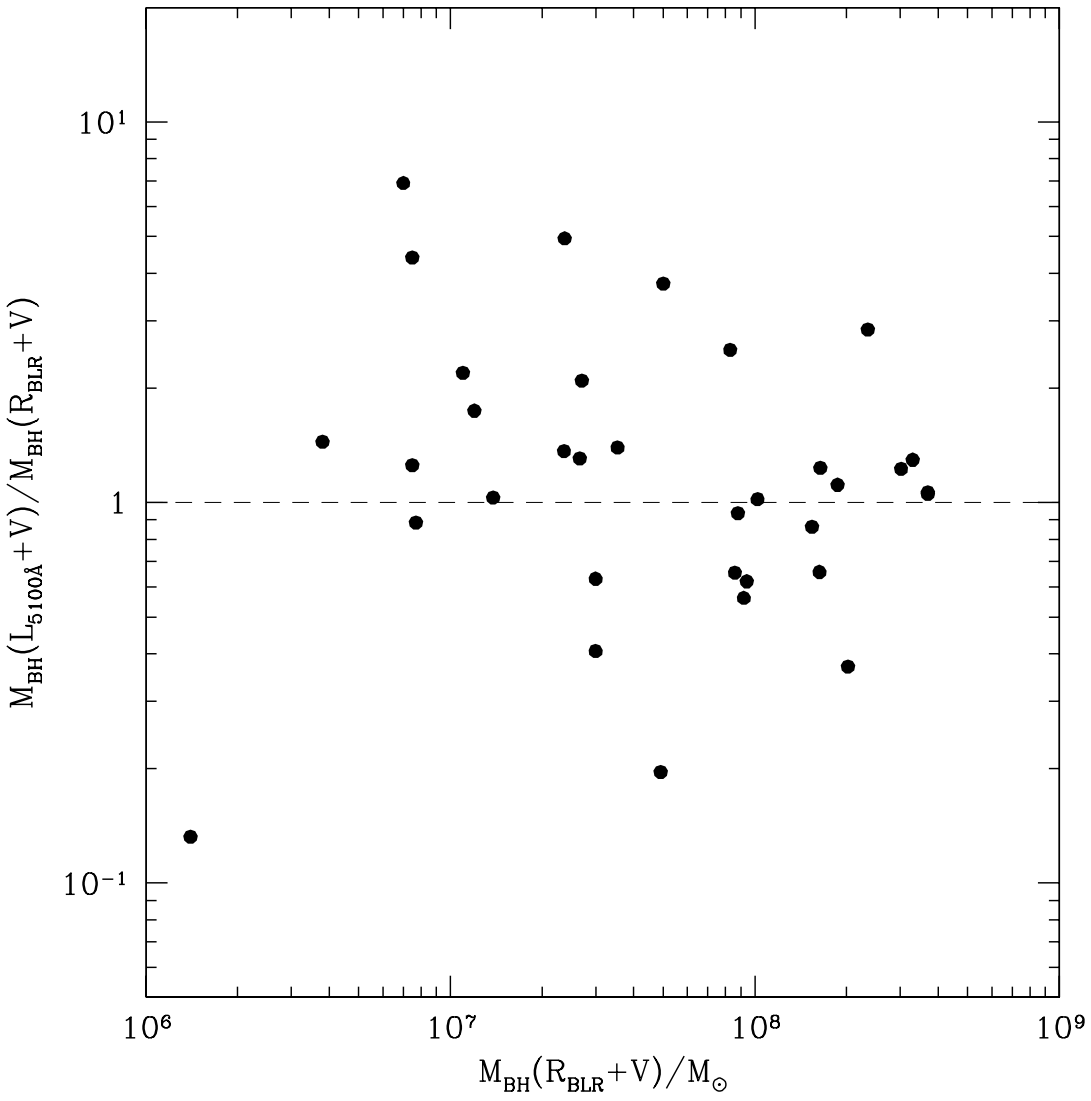

Fig. 2.— Comparison of black hole masses calculated using two different estimates of broad-line region (BLR) size — from reverberation mapping and from the $R_{BLR} - L_{5100\mathrm{A}^\circ}$ relation of Kaspi et al. (2000) — combined with the rms velocity of the $H\beta$ line (assuming $f = \sqrt{3}/2$ in Eq. 2, corresponding to random isotropic orbits). Relative uncertainties are as large as an order of magnitude, and come mainly from the large scatter in the size–luminosity relation. The unknown orbits add another factor of 3 or more uncertainty in the black hole mass (not represented in this plot).

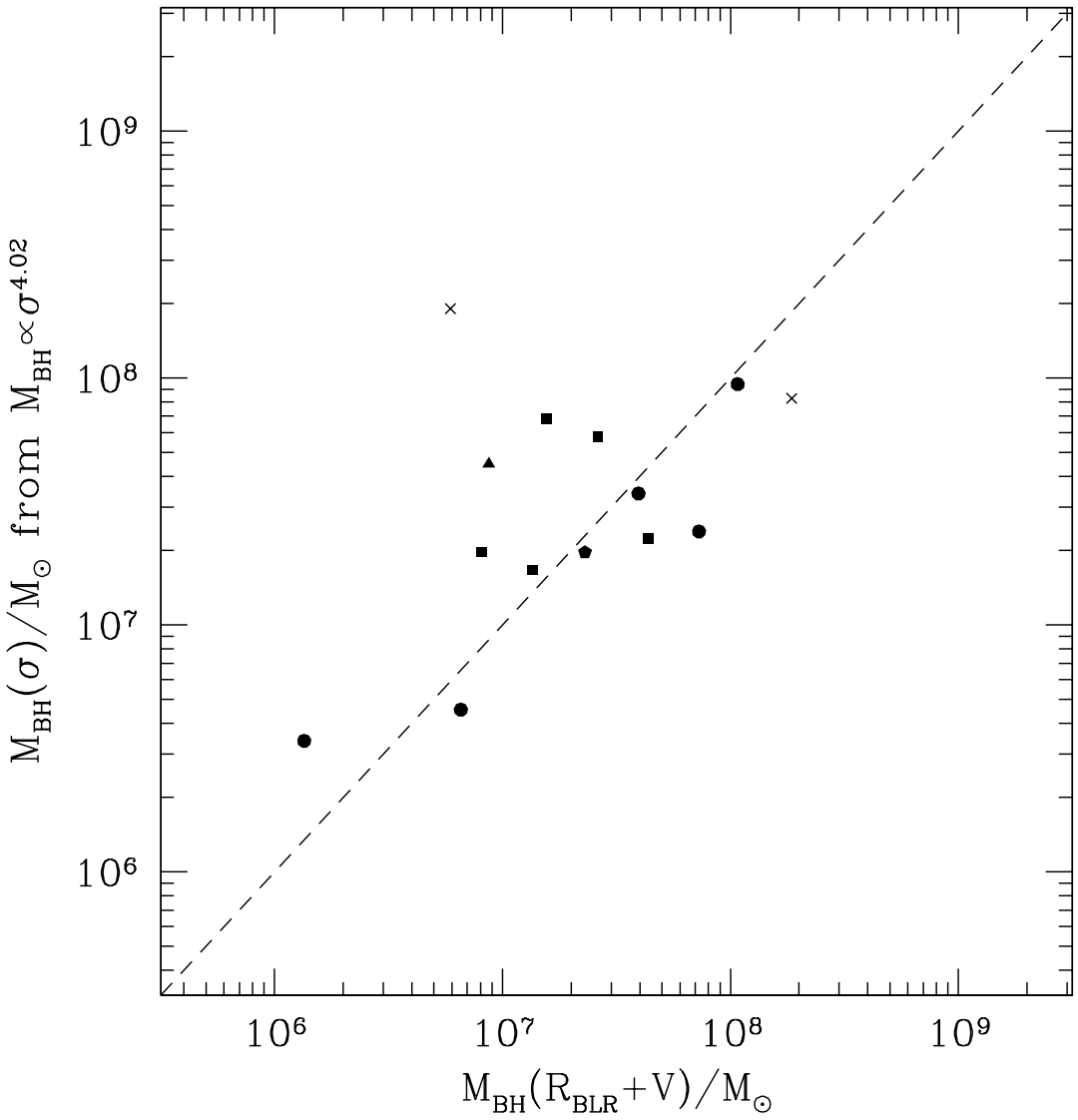

Fig. 3.— Comparison of two completely independent estimates of black hole mass, one from the stellar velocity dispersion correlation, $M_{BH} \propto \sigma^{4.02}$, and the other from reverberation mapping. Apart from one discordant object, IC 4329, the two masses agree well, with dispersion less than 50%. Reverberation masses are based on the values in Kaspi et al. (2000; log mean of two values from rms and mean velocity), Ho (1999; *triangle*), and Onken & Peterson (2002; *crosses*). Stellar velocity dispersion masses are from Nelson (1995; *squares*), Ferrarese et al. (2001; *circles*), Oliva et al. (1995; *triangle*), Di Nella et al. (1995; *pentagon*), and Oliva et al. (1999; *crosses*).

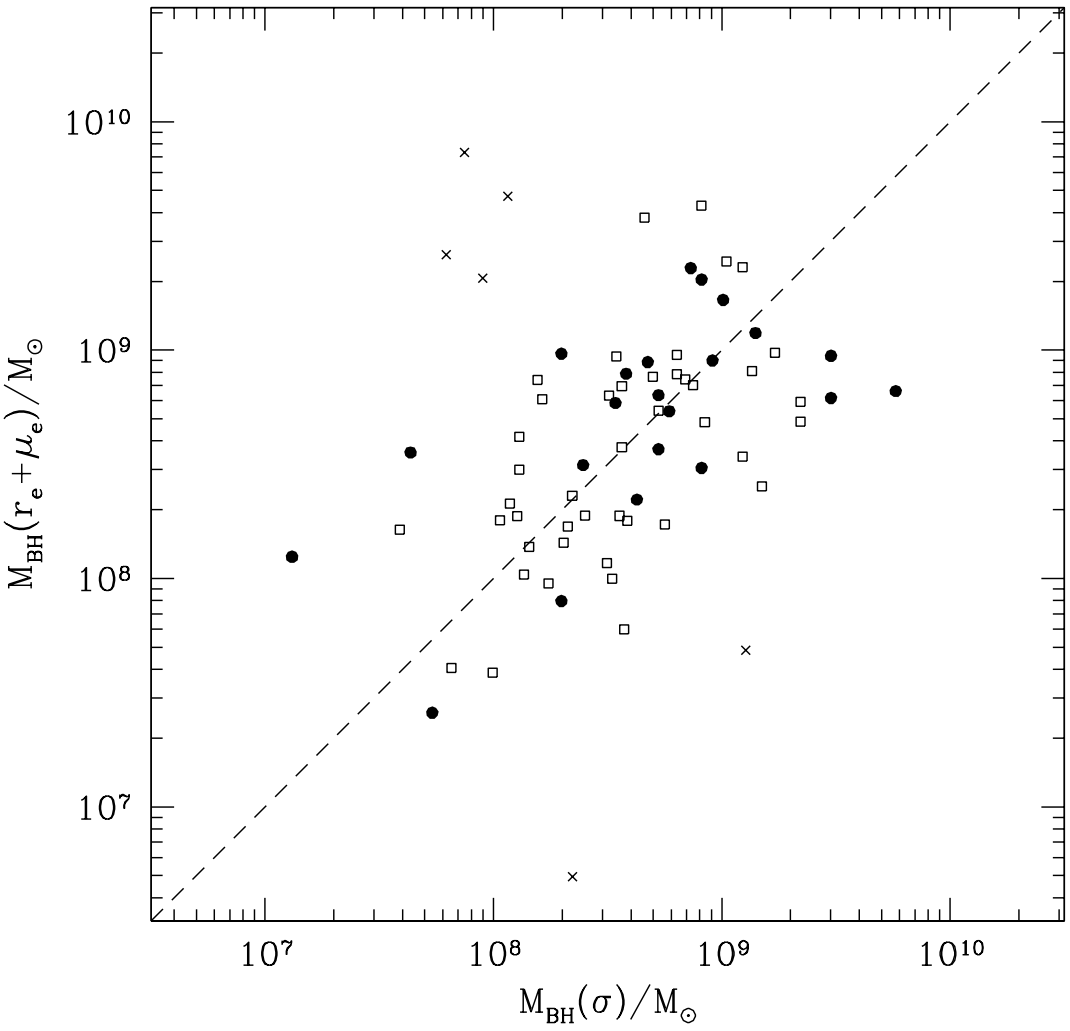

Fig. 4.— Black hole masses estimated from the correlation with stellar velocity dispersion, for the Bettoni et al. (2001) sample of radio galaxies. The plot compares $M_{BH}(r_e+\mu_e)$, derived from an indirect estimate of σ based on measured r_e and μ_e) and the fundamental plane relation, to $M_{BH}(\sigma)$, derived from direct measurements of the stellar velocity dispersion. Measurements of σ include a homogeneous set of 22 new measurements presented by Bettoni et al. (*filled circles*) and another 50 measurements (*open squares*) assembled by Bettoni et al. from the literature; the latter have larger scatter probably because they had to be transformed in color (from V to R) and corrected for different apertures. Apart from 6 outliers (*crosses*), most values agree well, with an rms dispersion of less than a factor of 4.

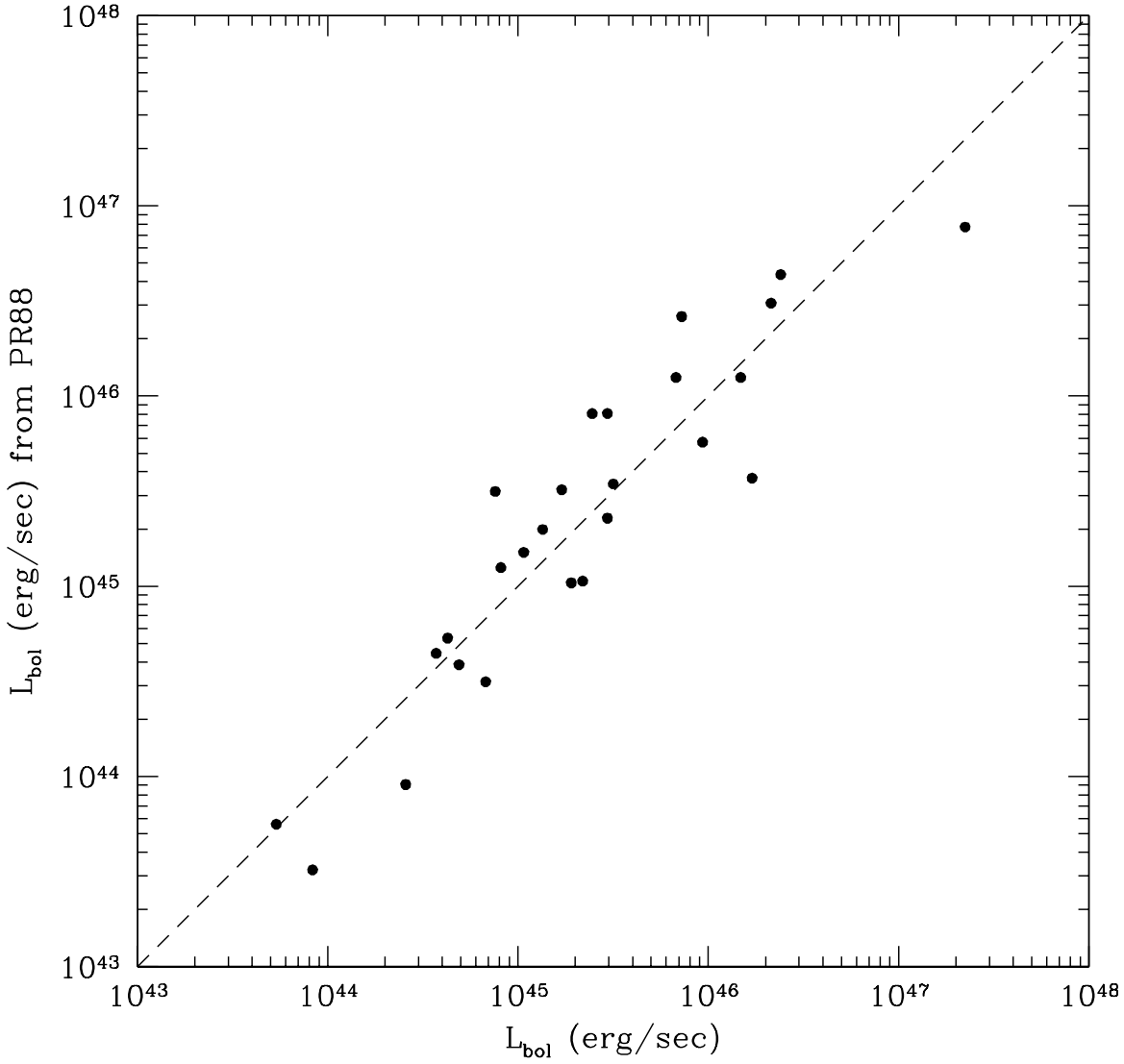

Fig. 5.— Comparison of bolometric luminosity measurements from present paper to those of Padovani & Rafanelli 1988, for the 26 AGN found in both samples. The two values are consistent; the very slightly smaller values found by Padovani & Rafanelli are due to the more limited spectral range over which they integrated the flux.

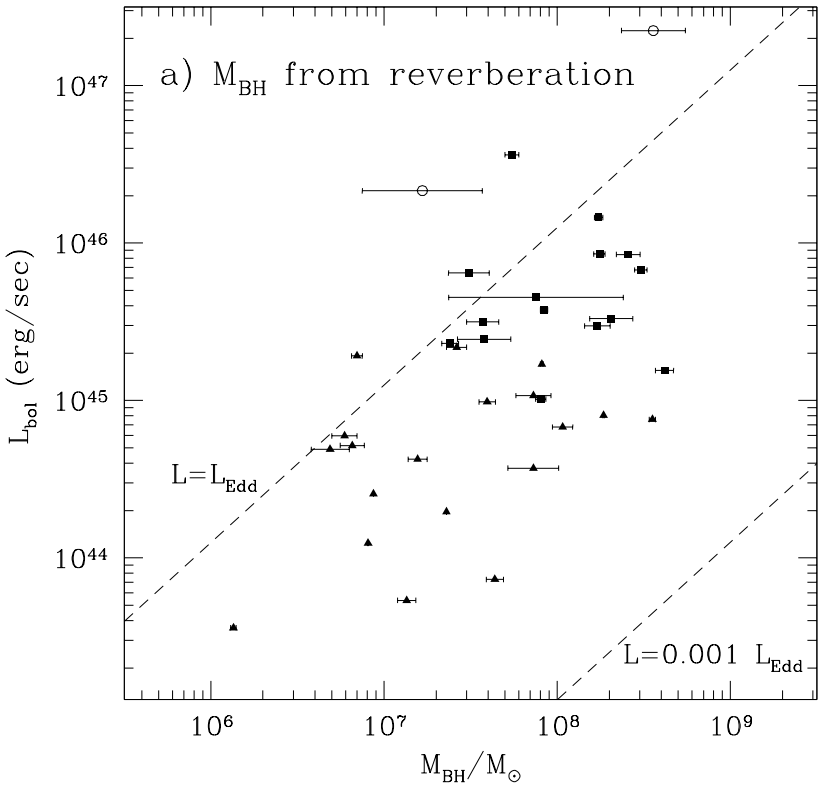

Fig. 6.— *a:* Bolometric luminosity versus black hole mass for 36 reverberation-mapped AGN. The range in luminosity is roughly two orders of magnitude for a given black hole mass. The mass plotted is the logarithmic mean from estimates with different velocity assumptions (measuring the FWHM from the rms spectrum or using the mean of FWHM measured from individual spectra), with the error bar indicating the range. *b:* The same mass–luminosity relation for Seyfert galaxies for which black hole masses have been estimated from measured stellar velocity dispersions (Eq. 4). The bolometric luminosities of these Seyferts span 1-3 orders of magnitude for a given black hole mass. The error bar indicates the uncertainty in black hole mass due to the measurement error in σ. *c:* Mass–luminosity relation for 139 quasars whose black hole masses have been estimated using line widths plus the optical luminosity to infer broad-line-region size (McLure & Dunlop 2001, Laor 2001, Gu et al. 2001). A correlation is induced by the mass determination if bolometric luminosity is linearly correlated with optical luminosity; the correlation should follow $M_{BH} \propto L_{bol}^{0.7}$ (*thick line*). Symbols are *open circles:* radio-loud quasars; *filled squares:* radio-quiet quasars; *filled triangles:* Seyfert 1; *filled pentagons:* Seyfert 2.

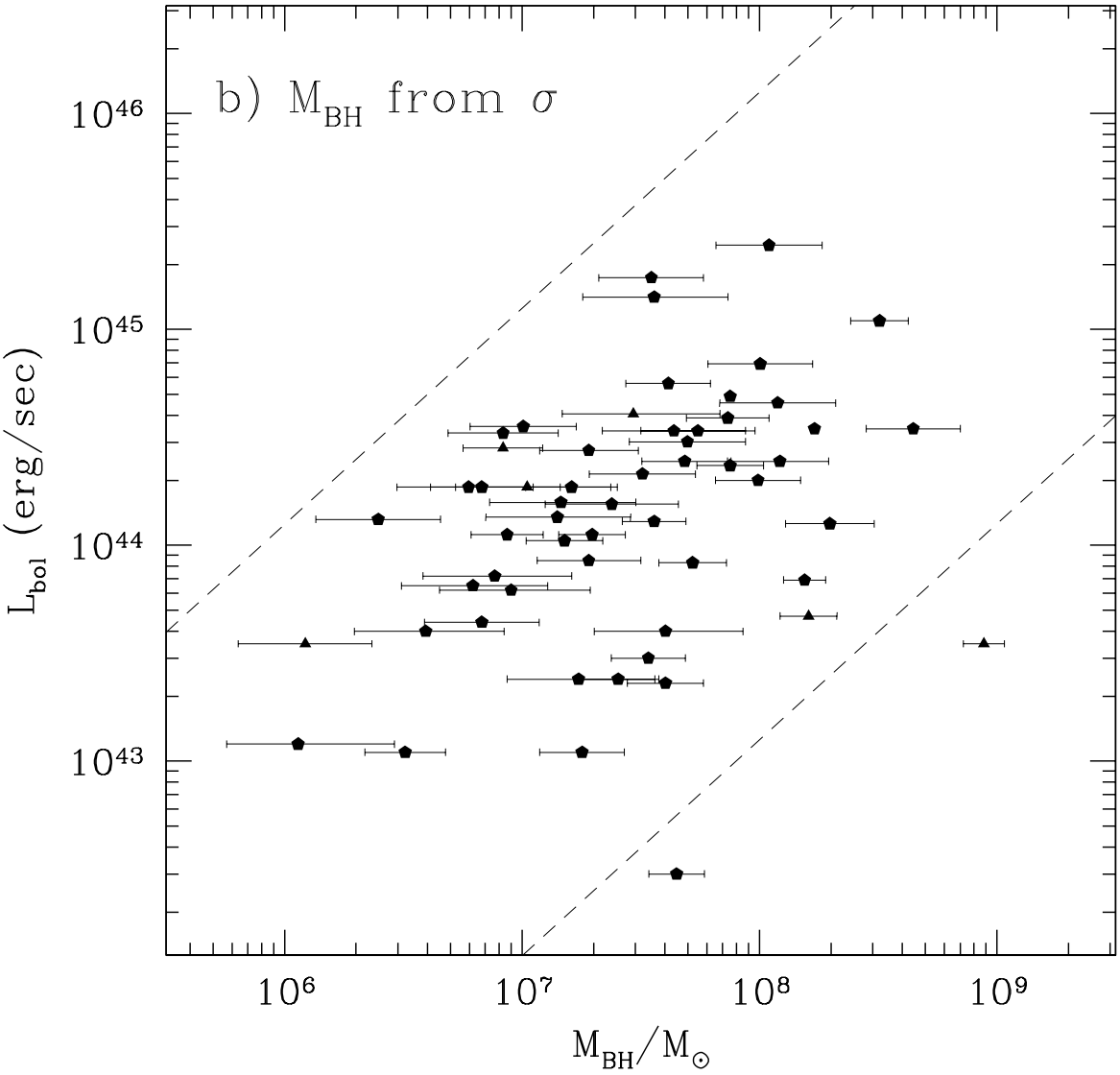
b) M_{BH} from σ
10^{46}
10^{45}
10^{44}
10^{43}
L_{bol} (erg/sec)
10^6
10^7
10^8
10^9
$M_{BH}/M_\odot$

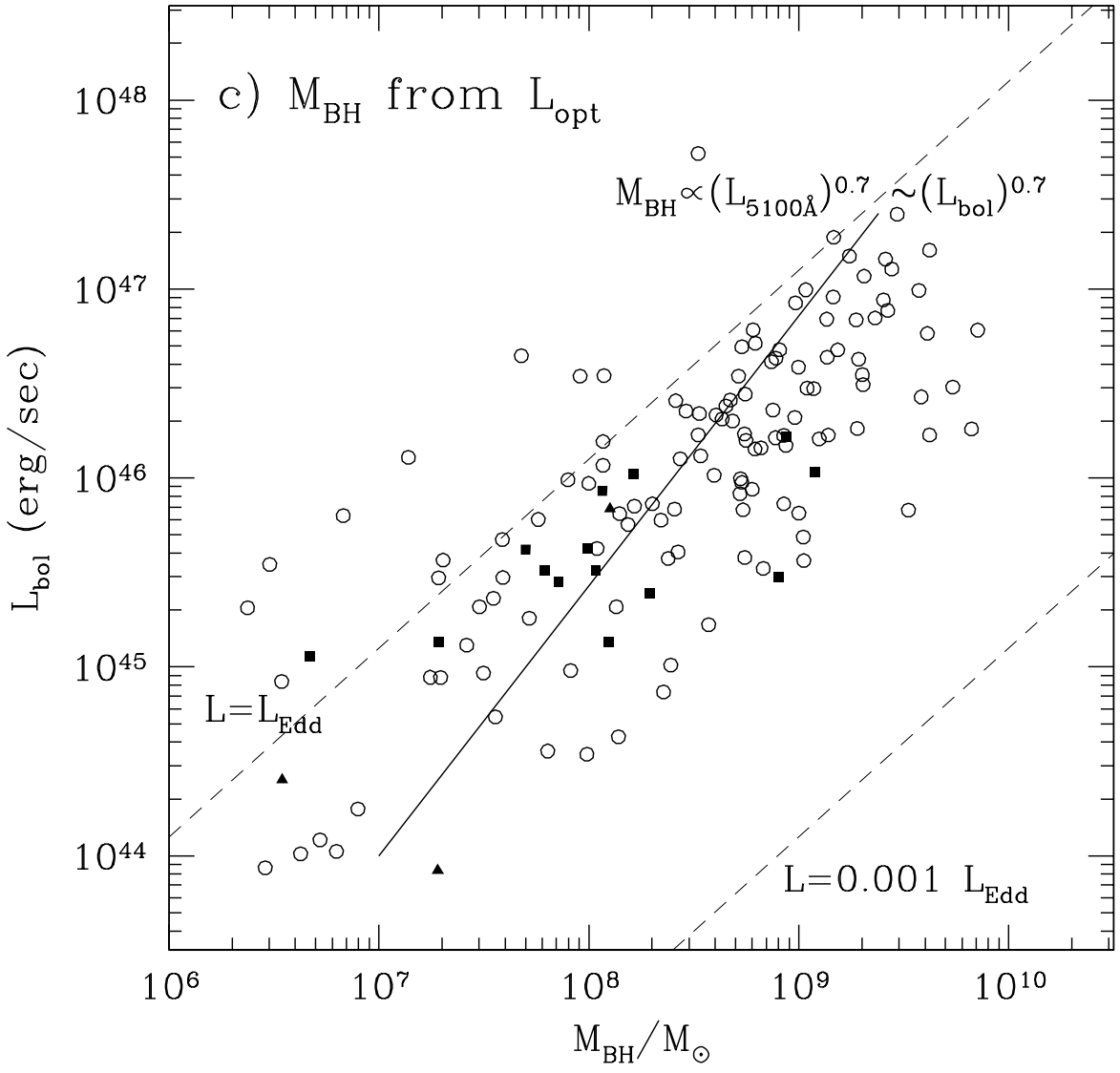
c) M_{BH} from L_{opt}
$M_{BH} \propto (L_{5100Å})^{0.7} \sim (L_{bol})^{0.7}$
$L = L_{Edd}$
$L = 0.001\ L_{Edd}$
L_{bol} (erg/sec)
$M_{BH}/M_{\odot}$
10^{44}
10^{45}
10^{46}
10^{47}
10^{48}
10^{6}
10^{7}
10^{8}
10^{9}
10^{10}

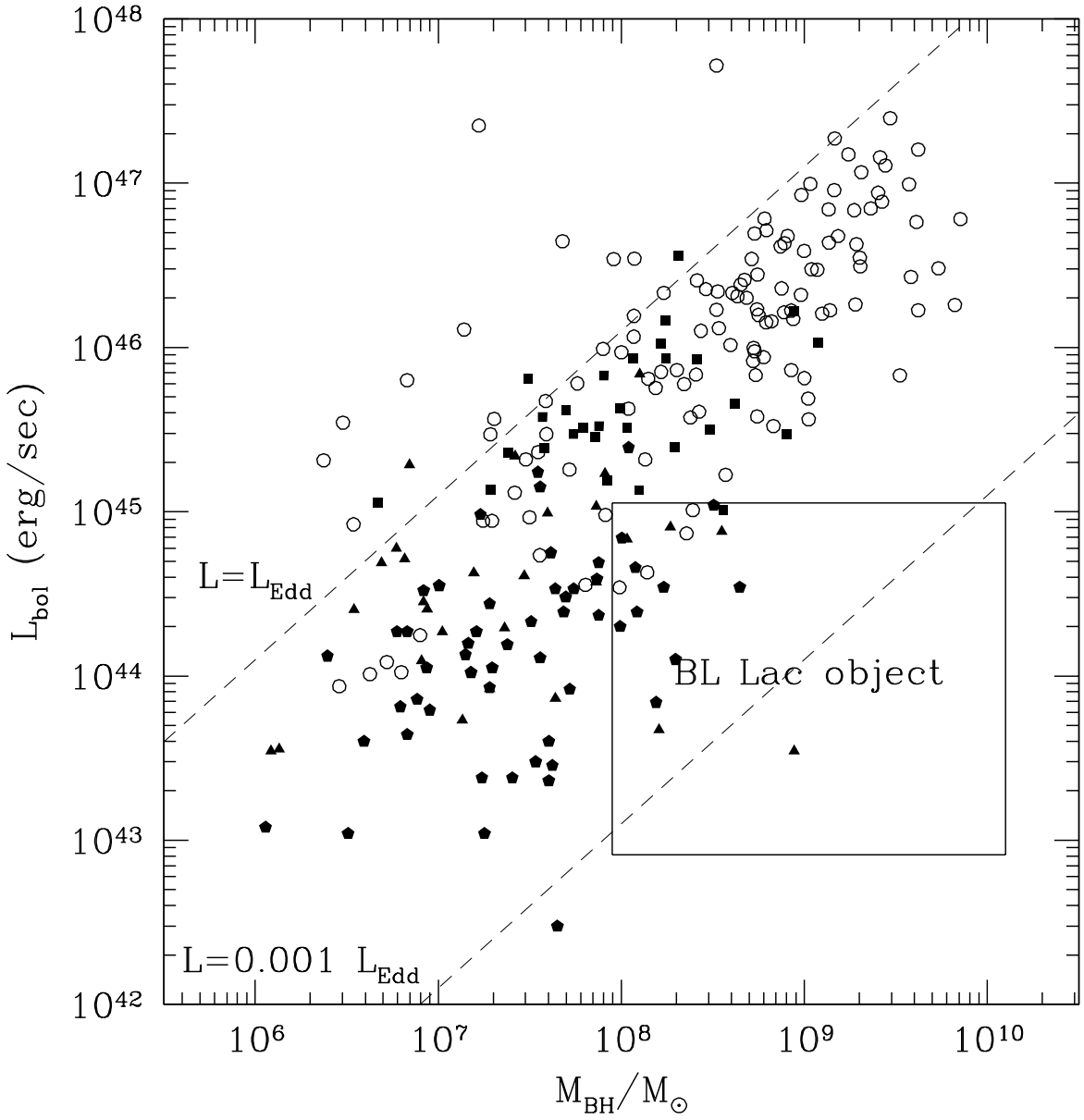

Fig. 7.— Bolometric luminosity versus black hole mass for 234 AGN. There is little if any correlation. For a given black hole mass, there is a large range of bolometric luminosities, spanning three or more orders of magnitude. The Eddington limit defines an approximate upper limit to the luminosity, but the absence of objects from the lower right of the diagram (low luminosity, high mass AGN) is a selection effect. For example, this part of the diagram would be occupied by BL Lac objects and low-luminosity radio galaxies. The inner box indicates the approximate location of BL Lac objects (see text). The symbols are the same as Figure 6.

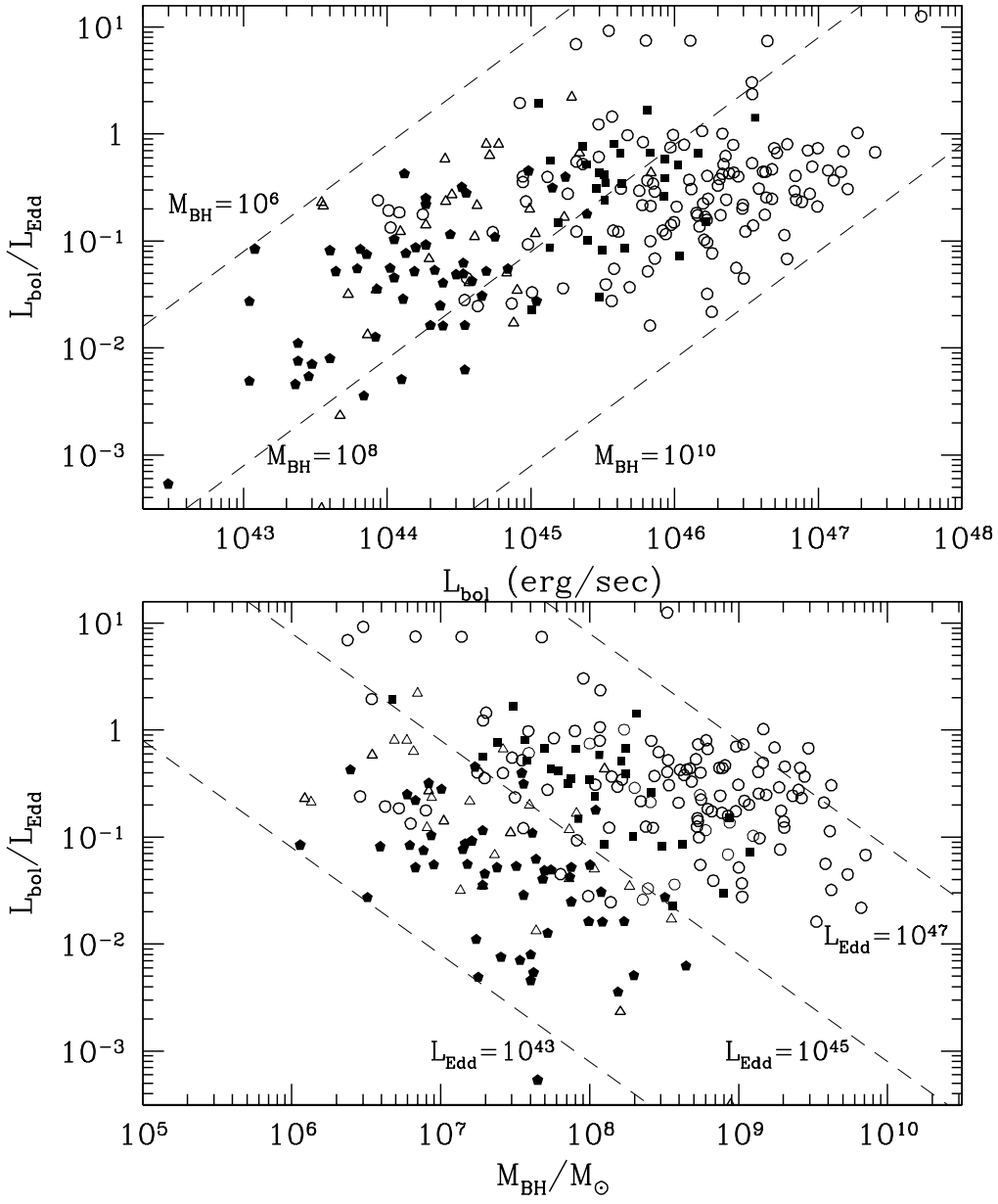

Fig. 8.— Eddington ratio versus bolometric luminosity (*top panel*) and versus black hole mass (*bottom panel*). The range of Eddington ratios is roughly two orders of magnitude over most of the observed luminosity or black hole mass ranges. The apparent deficit of high-luminosity objects with low Eddington ratios (i.e., with black holes in the range $10^8 < M_{\rm BH}/M_\odot < 10^{10}$) and of low-luminosity objects with high Eddington ratios, as well as the absence of higher and lower luminosity AGN in the lower panel, are likely caused by selection effects (see text). The symbols are the same as Figure 6.

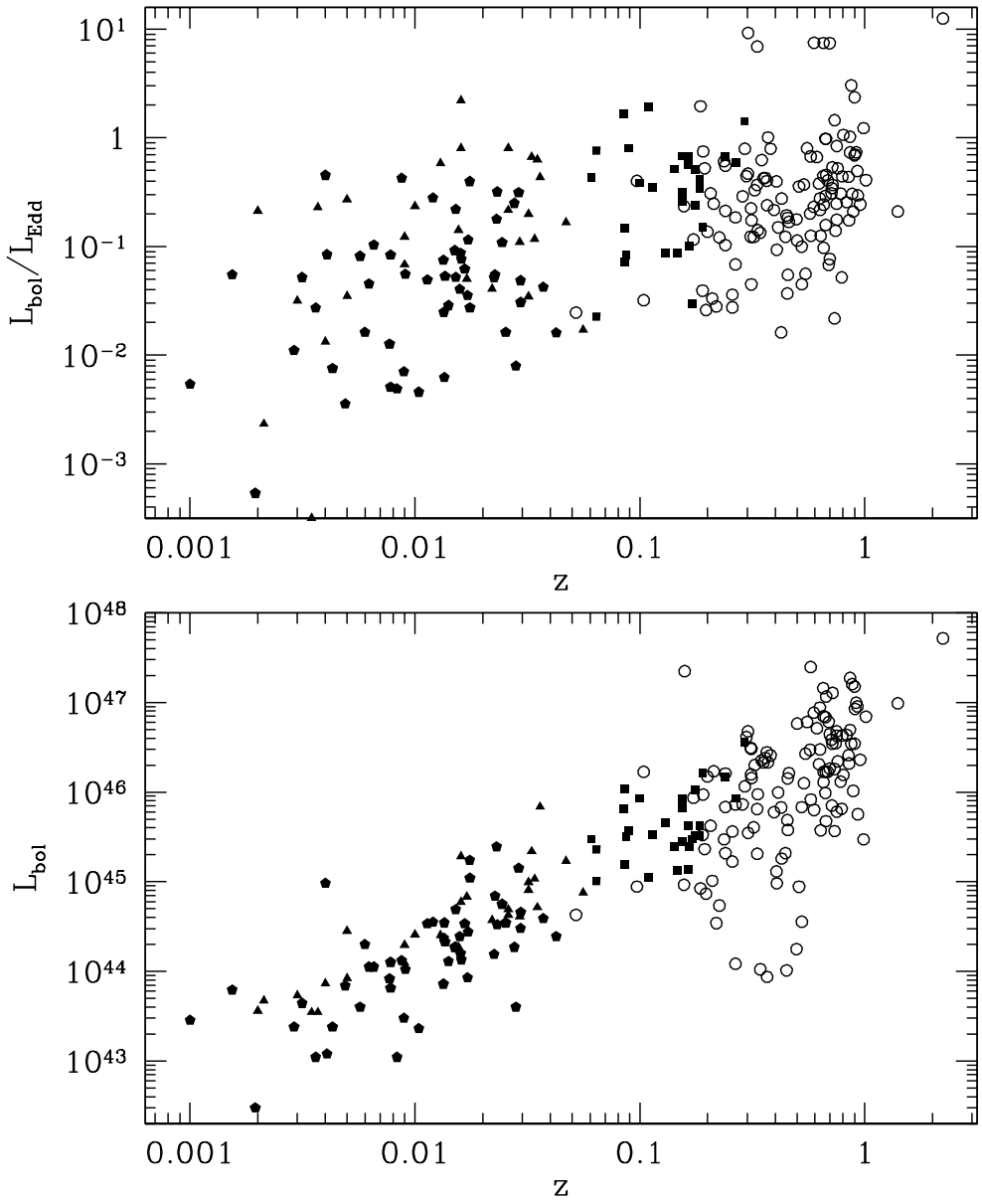

Fig. 9.— Eddington ratio (*top panel*) and bolometric luminosity (*bottom panel*) versus redshift. The Eddington ratio ranges from 0.001 to 1 at low redshifts, and from 0.01 to 10 at higher redshifts; although this represents a broad trend toward higher ratios at higher luminosities, the scatter is large and selection effects are significant. The bottom panel shows clearly selection effects that are limiting the sample of AGN: the flux limit (lower envelope) and the steepness of the luminosity function, which describes how luminous objects more rare and thus are found only in larger volumes, i.e., at higher redshifts (upper envelope). These effects cause the broad distribution of Eddington ratios in the top panel to be bounded, most notably in the lower left. Even at that, the Eddington ratio has a broad range of values at every redshift. The symbols are the same as Figure 6.

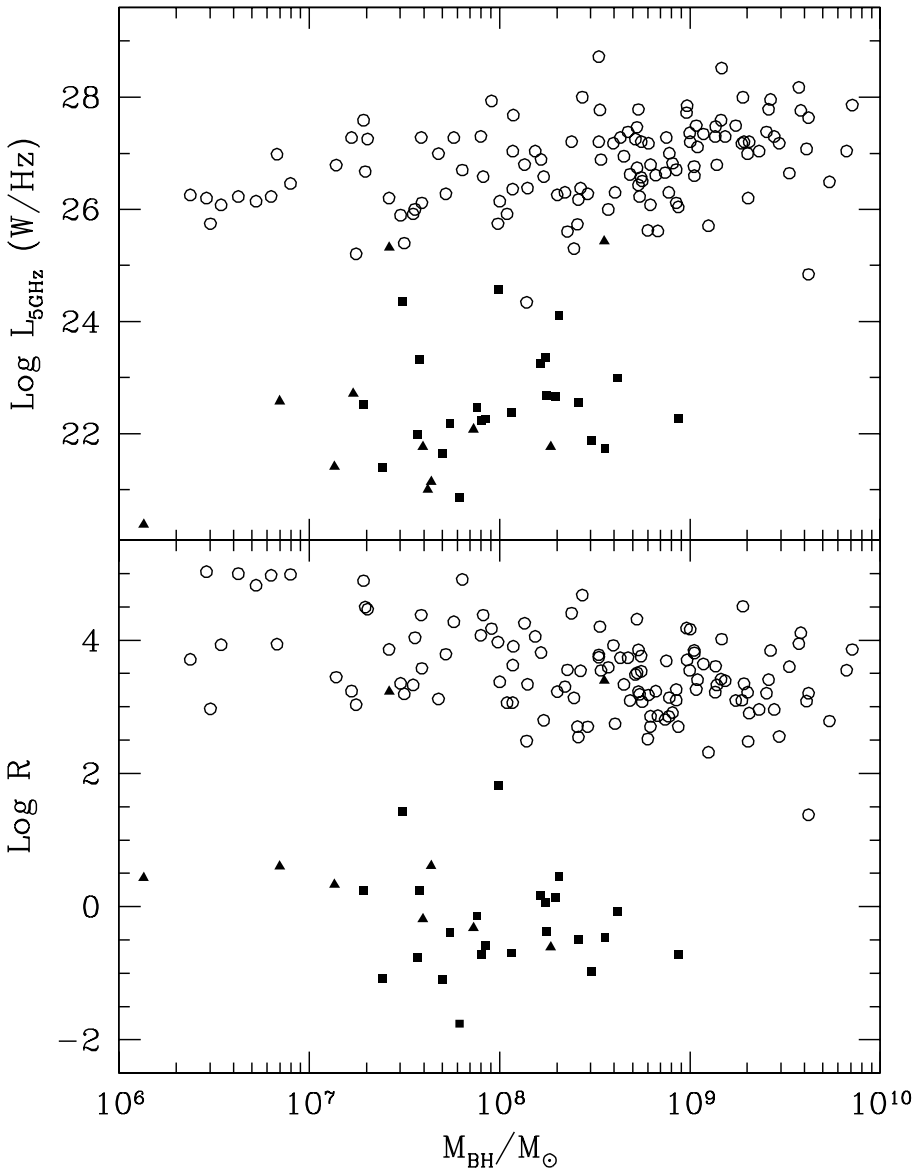

Fig. 10.— Dependence of radio properties on black hole mass. *Top panel:* Radio luminosity at 5 GHz versus black hole mass for 157 AGN. Both radio-quiet and radio-loud quasars span a large range in black hole masses. The highest mass objects plotted do have the highest radio luminosities but objects that would fall in the lower right of the plot (BL Lac objects and radio galaxies) have been excluded (due to the difficulty in accurately estimating bolometric luminosity). Note also that some of the highest radio power sources have some of the lowest black hole masses. *Bottom panel:* Radio loudness (f_{5GHz}/f_{opt}) versus black hole mass for the same 157 AGN. There is little dependence of radio loudness on mass, apart from an absence of the highest mass black holes in the radio-quiet population; present data are not sufficient to determine whether this absence is a real effect or due to sample selection and observational bias. The symbols are the same as Figure 6.

Table 1. Summary of Black Hole Mass Estimates

Method	Number	References
Spatially resolved kinematics	2	Greenhill et al. 1996, Miyoshi et al. 1995
Reverberation mapping	36	Ho 1999, Kaspi et al. 2000, Onken & Peterson 2002
L_{opt}–R_{BLR} relation	139	McLure & Dunlop 2001, Laor 2001, Gu et al. 2001, Oshlack et al. 2002
M_{BH}–σ relation	33	Wu & Han 2001, Barth et al. 2002, Falomo et al. 2002
	108	This work
Fundamental plane	59	This work

Table 2. Black Hole Masses from Spatially Resolved Kinematics

Name	z	L_{bol}		M_{BH}	ref.	Type
NGC 1068	0.004	44.98	I	7.23	1	SY2
NGC 4258	0.001	43.45	I	7.62	2	SY2

[a] Column (1) Name, (2) redshift, (3) log of the bolometric luminosity (ergs s^{-1}), (4) method for bolometric luminosity estimation (I: flux integration; F: SED fitting), (5) log of black hole mass in solar masses estimated from maser kinematics, (6) reference for black hole mass estimation, and (7) AGN type.

References. — (1) Greenhill et al. (1996), (2) Miyoshi et al. (1995).

Table 3. Black Hole Masses from Reverberation Mapping

Name	z	L_{bol}		M_{BH}	ref.	Type
3C 120	0.033	45.34	I	7.42	1	SY1
3C 390.3	0.056	44.88	I	8.55	1	SY1
Akn 120	0.032	44.91	I	8.27	1	SY1
F 9	0.047	45.23	F	7.91	1	SY1
IC 4329A	0.016	44.78	I	6.77	1	SY1
Mrk 79	0.022	44.57	I	7.86	1	SY1
Mrk 110	0.035	44.71	F	6.82	1	SY1
Mrk 335	0.026	44.69	I	6.69	1	SY1
Mrk 509	0.034	45.03	I	7.86	1	SY1
Mrk 590	0.026	44.63	I	7.20	1	SY1
Mrk 817	0.032	44.99	I	7.60	1	SY1
NGC 3227	0.004	43.86	I	7.64	1	SY1
NGC 3516	0.009	44.29	I	7.36	3	SY1
NGC 3783	0.010	44.41	I	6.94	2	SY1
NGC 4051	0.002	43.56	I	6.13	1	SY1
NGC 4151	0.003	43.73	I	7.13	1	SY1
NGC 4593	0.009	44.09	I	6.91	3	SY1
NGC 5548	0.017	44.83	I	8.03	1	SY1
NGC 7469	0.016	45.28	I	6.84	1	SY1
PG 0026+129	0.142	45.39	I	7.58	1	RQQ
PG 0052+251	0.155	45.93	F	8.41	1	RQQ
PG 0804+761	0.100	45.93	F	8.24	1	RQQ
PG 0844+349	0.064	45.36	F	7.38	1	RQQ
PG 0953+414	0.239	46.16	F	8.24	1	RQQ
PG 1211+143	0.085	45.81	F	7.49	1	RQQ
PG 1229+204	0.064	45.01	I	8.56	1	RQQ
PG 1307+085	0.155	45.83	F	7.90	1	RQQ
PG 1351+640	0.087	45.50	I	8.48	1	RQQ
PG 1411+442	0.089	45.58	F	7.57	1	RQQ
PG 1426+015	0.086	45.19	I	7.92	1	RQQ
PG 1613+658	0.129	45.66	I	8.62	1	RQQ

Table 3—Continued

Name	z	L_{bol}		M_{BH}	ref.	Type
PG 1617+175	0.114	45.52	F	7.88	1	RQQ
PG 1700+518	0.292	46.56	F	8.31	1	RQQ
PG 2130+099	0.061	45.47	I	7.74	1	RQQ
PG 1226+023	0.158	47.35	I	7.22	1	RLQ
PG 1704+608	0.371	46.33	I	8.23	1	RLQ

[a] Column (1) Name, (2) redshift, (3) log of the bolometric luminosity (ergs s^{-1}), (4) method for bolometric luminosity estimation (I: flux integration; F: SED fitting), (5) black hole mass estimate from reverberation mapping (for Kaspi et al. (2000) sample, where black hole mass is log mean of rms FWHM and mean FWHM mass, in solar masses), (6) reference for black hole mass estimation, and (7) AGN type.

References. — (1) Kaspi et al. (2000), (2) Onken & Peterson (2002), (3) Ho (1999).

Table 4. Black Hole Masses from Optical Luminosity

Name	z	L_{bol}		M_{BH}	ref.	Type
Mrk 841	0.036	45.84	I	8.10	1	SY1
NGC 4253	0.013	44.40	I	6.54	1	SY1
NGC 6814	0.005	43.92	I	7.28	1	SY1
0054+144	0.171	45.47	F	8.90	2	RQQ
0157+001	0.164	45.62	F	7.70	2	RQQ
0204+292	0.109	45.05	F	6.67	2	RQQ
0205+024	0.155	45.45	F	7.86	2	RQQ
0244+194	0.176	45.51	F	8.03	2	RQQ
0923+201	0.190	46.22	F	8.94	2	RQQ
1012+008	0.185	45.51	F	7.79	2	RQQ
1029-140	0.086	46.03	F	9.08	2	RQQ
1116+215	0.177	46.02	F	8.21	2	RQQ
1202+281	0.165	45.39	F	8.29	2	RQQ
1309+355	0.184	45.63	F	8.00	2	RQQ
1402+261	0.164	45.13	F	7.29	2	RQQ
1444+407	0.267	45.93	F	8.06	2	RQQ
1635+119	0.146	45.13	F	8.10	2	RQQ
0022-297	0.406	44.98	F	7.91	3	RLQ
0024+348	0.333	45.31	F	6.37	3	RLQ
0056-001	0.717	46.54	F	8.71	3	RLQ
0110+495	0.395	45.78	F	8.34	3	RLQ
0114+074	0.343	44.02	F	6.80	4	RLQ
0119+041	0.637	45.57	F	8.38	3	RLQ
0133+207	0.425	45.83	F	9.52	3	RLQ
0133+476	0.859	46.69	F	8.73	3	RLQ
0134+329	0.367	46.44	F	8.74	3	RLQ
0135-247	0.831	46.64	F	9.13	3	RLQ
0137+012	0.258	45.22	F	8.57	2	RLQ
0153-410	0.226	44.74	F	7.56	4	RLQ
0159-117	0.669	46.84	F	9.27	3	RLQ
0210+860	0.186	44.92	F	6.54	3	RLQ
0221+067	0.510	44.94	F	7.29	4	RLQ
0237-233	2.224	47.72	F	8.52	3	RLQ

Table 4—Continued

Name	z	L_{bol}		M_{BH}	ref.	Type
0327-241	0.888	46.01	F	8.60	4	RLQ
0336-019	0.852	46.32	F	8.98	3	RLQ
0403-132	0.571	46.47	F	9.07	3	RLQ
0405-123	0.574	47.40	F	9.47	3	RLQ
0420-014	0.915	47.00	F	9.03	3	RLQ
0437+785	0.454	46.15	F	8.79	3	RLQ
0444+634	0.781	46.12	F	8.53	3	RLQ
0454-810	0.444	45.32	F	8.13	3	RLQ
0454+066	0.405	45.12	F	7.42	4	RLQ
0502+049	0.954	46.36	F	8.88	4	RLQ
0514-459	0.194	45.36	F	7.55	3	RLQ
0518+165	0.759	46.34	F	8.53	3	RLQ
0538+498	0.545	46.43	F	9.58	3	RLQ
0602-319	0.452	45.69	F	9.02	3	RLQ
0607-157	0.324	46.30	F	8.68	3	RLQ
0637-752	0.654	47.16	F	9.41	3	RLQ
0646+600	0.455	45.58	F	8.74	3	RLQ
0723+679	0.846	46.41	F	8.67	3	RLQ
0736+017	0.191	45.97	F	8.00	2	RLQ
0738+313	0.631	46.94	F	9.40	3	RLQ
0809+483	0.871	46.54	F	7.96	3	RLQ
0838+133	0.684	46.23	F	8.52	3	RLQ
0906+430	0.668	45.99	F	7.90	3	RLQ
0912+029	0.427	45.26	F	7.72	4	RLQ
0921-213	0.052	44.63	F	8.14	4	RLQ
0923+392	0.698	46.26	F	9.28	3	RLQ
0925-203	0.348	46.35	F	8.46	4	RLQ
0953+254	0.712	46.59	F	9.00	3	RLQ
0954+556	0.901	46.54	F	8.07	3	RLQ
1004+130	0.240	46.21	F	9.10	2	RLQ
1007+417	0.612	46.71	F	8.79	3	RLQ
1016-311	0.794	46.63	F	8.89	4	RLQ
1020-103	0.197	44.87	F	8.36	2	RLQ

Table 4—Continued

Name	z	L_{bol}		M_{BH}	ref.	Type
1034-293	0.312	46.20	F	8.75	3	RLQ
1036-154	0.525	44.55	F	7.80	4	RLQ
1045-188	0.595	45.80	F	6.83	3	RLQ
1100+772	0.311	46.49	F	9.31	3	RLQ
1101-325	0.355	46.33	F	8.61	4	RLQ
1106+023	0.157	44.97	F	7.50	4	RLQ
1107-187	0.497	44.25	F	6.90	4	RLQ
1111+408	0.734	46.26	F	9.82	3	RLQ
1128-047	0.266	44.08	F	6.72	4	RLQ
1136-135	0.554	46.78	F	8.78	3	RLQ
1137+660	0.656	46.85	F	9.36	3	RLQ
1150+497	0.334	45.98	F	8.73	3	RLQ
1151-348	0.258	45.56	F	9.02	3	RLQ
1200-051	0.381	46.41	F	8.41	4	RLQ
1202-262	0.789	45.81	F	9.00	3	RLQ
1217+023	0.240	45.83	F	8.41	2	RLQ
1237-101	0.751	46.63	F	9.28	4	RLQ
1244-255	0.633	46.48	F	9.04	3	RLQ
1250+568	0.321	45.61	F	8.42	3	RLQ
1253-055	0.536	46.10	F	8.43	3	RLQ
1254-333	0.190	45.52	F	8.83	4	RLQ
1302-102	0.286	45.86	F	8.30	2	RLQ
1352-104	0.332	45.81	F	8.15	4	RLQ
1354+195	0.720	47.11	F	9.44	3	RLQ
1355-416	0.313	46.48	F	9.73	3	RLQ
1359-281	0.803	46.19	F	8.07	4	RLQ
1450-338	0.368	43.94	F	6.46	4	RLQ
1451-375	0.314	46.16	F	8.82	3	RLQ
1458+718	0.905	46.93	F	8.98	3	RLQ
1509+022	0.219	44.54	F	7.99	4	RLQ
1510-089	0.361	46.38	F	8.65	3	RLQ
1545+210	0.266	45.86	F	8.93	2	RLQ
1546+027	0.412	46.00	F	8.72	3	RLQ

Table 4—Continued

Name	z	L_{bol}		M_{BH}	ref.	Type
1555-140	0.097	44.94	F	7.25	4	RLQ
1611+343	1.401	46.99	F	9.57	3	RLQ
1634+628	0.988	45.47	F	7.28	3	RLQ
1637+574	0.750	46.68	F	9.18	3	RLQ
1641+399	0.594	46.89	F	9.42	3	RLQ
1642+690	0.751	45.78	F	7.76	3	RLQ
1656+053	0.879	47.21	F	9.62	3	RLQ
1706+006	0.449	44.01	F	6.63	4	RLQ
1721+343	0.206	45.63	F	8.04	3	RLQ
1725+044	0.293	46.07	F	8.07	3	RLQ
1726+455	0.714	45.85	F	8.22	3	RLQ
1828+487	0.691	46.78	F	9.85	3	RLQ
1849+670	0.657	46.23	F	9.14	3	RLQ
1856+737	0.460	46.21	F	8.89	3	RLQ
1928+738	0.302	46.68	F	8.91	3	RLQ
1945+725	0.303	45.54	F	6.48	3	RLQ
1954-388	0.626	46.31	F	8.63	4	RLQ
2004-447	0.240	45.32	F	7.48	4	RLQ
2043+749	0.104	46.23	F	9.62	3	RLQ
2059+034	1.012	46.84	F	9.13	4	RLQ
2111+801	0.524	45.83	F	8.73	3	RLQ
2120+099	0.932	45.75	F	8.19	4	RLQ
2128-123	0.501	46.76	F	9.61	3	RLQ
2135-147	0.200	46.17	F	8.94	2	RLQ
2141+175	0.213	46.23	F	8.74	2	RLQ
2143-156	0.698	46.65	F	7.68	4	RLQ
2155-152	0.672	45.67	F	7.59	3	RLQ
2201+315	0.298	46.62	F	8.87	3	RLQ
2216-038	0.901	47.17	F	9.24	3	RLQ
2218+395	0.655	46.11	F	7.14	3	RLQ
2247+140	0.237	45.47	F	7.59	2	RLQ
2251+158	0.859	47.27	F	9.17	3	RLQ
2255-282	0.926	46.96	F	9.16	3	RLQ

Table 4—Continued

Name	z	L_{bol}		M_{BH}	ref.	Type
2311+469	0.741	46.55	F	9.30	3	RLQ
2329-415	0.671	46.22	F	8.93	4	RLQ
2342+821	0.735	45.56	F	7.31	3	RLQ
2344+092	0.673	47.07	F	9.31	3	RLQ
2345-167	0.576	45.92	F	8.72	3	RLQ
2349-014	0.173	45.94	F	8.78	2	RLQ
2355-082	0.210	45.01	F	8.39	2	RLQ

[a] Column (1) Name, (2) redshift, (3) log of the bolometric luminosity (ergs s^{-1}), (4) method for bolometric luminosity estimation (I: flux integration; F: SED fitting), (5) log of the black hole mass in solar masses, estimated using $L_{opt} - M_{BH}$ relation (Eq. 3), (6) reference for optical luminosity, (7) AGN type.

References. — (1) Laor 2001, (2) McLure & Dunlop 2001, (3) Gu et al. 2001, (4) Oshlack et al. 2002.

Table 5. Black Hole Masses from Observed Stellar Velocity Dispersions

Name	z	σ	ref.	M_{BH}	L_{bol}		Type
NGC 1566	0.005	100.	N	6.92	44.45	I	SY1
NGC 2841	0.002	209.	N	8.21	43.67	I	SY1
NGC 3982	0.004	62.	N	6.09	43.54	I	SY1
NGC 3998	0.003	319.	N	8.95	43.54	I	SY1
Mrk 10	0.029	137.	N	7.47	44.61	I	SY1
UGC 3223	0.016	106.	N	7.02	44.27	I	SY1
NGC 513	0.002	152.	N	7.65	42.52	I	SY2
NGC 788	0.014	140.	N	7.51	44.33	I	SY2
NGC 1052	0.005	207.	N	8.19	43.84	I	SY2
NGC 1275	0.018	248.	N	8.51	45.04	I	SY2
NGC 1320	0.009	116.	N	7.18	44.02	I	SY2
NGC 1358	0.013	173.	N	7.88	44.37	I	SY2
NGC 1386	0.003	120.	N	7.24	43.38	I	SY2
NGC 1667	0.015	173.	N	7.88	44.69	I	SY2
NGC 2110	0.008	220.	N	8.30	44.10	I	SY2
NGC 2273	0.006	124.	N	7.30	44.05	I	SY2
NGC 2992	0.008	158.	N	7.72	43.92	I	SY2
NGC 3185	0.004	61.	N	6.06	43.08	I	SY2
NGC 3362	0.028	92.	N	6.77	44.27	I	SY2
NGC 3786	0.009	142.	N	7.53	43.47	I	SY2
NGC 4117	0.003	95.	N	6.83	43.64	F	SY2
NGC 4339	0.004	132.	N	7.40	43.38	I	SY2
NGC 5194	0.002	102.	N	6.95	43.79	I	SY2
NGC 5252	0.023	190.	N	8.04	45.39	F	SY2
NGC 5273	0.004	79.	N	6.51	43.03	I	SY2
NGC 5347	0.008	93.	N	6.79	43.81	I	SY2
NGC 5427	0.009	74.	N	6.39	44.12	I	SY2
NGC 5929	0.008	121.	N	7.25	43.04	I	SY2
NGC 5953	0.007	101.	N	6.94	44.05	I	SY2
NGC 6104	0.028	148.	N	7.60	43.60	I	SY2
NGC 7213	0.006	185.	N	7.99	44.30	I	SY2

Table 5—Continued

Name	z	σ	ref.	M_{BH}	L_{bol}		Type
NGC 7319	0.023	130.	N	7.38	44.19	I	SY2
NGC 7603	0.030	194.	N	8.08	44.66	I	SY2
NGC 7672	0.013	98.	N	6.88	43.86	I	SY2
NGC 7682	0.017	123.	N	7.28	43.93	I	SY2
NGC 7743	0.006	83.	N	6.59	43.60	I	SY2
Mrk 1	0.016	115.	N	7.16	44.20	I	SY2
Mrk 3	0.014	269.	N	8.65	44.54	I	SY2
Mrk 78	0.037	172.	N	7.87	44.59	I	SY2
Mrk 270	0.010	148.	N	7.60	43.37	I	SY2
Mrk 348	0.015	118.	N	7.21	44.27	I	SY2
Mrk 533	0.029	144.	N	7.56	45.15	I	SY2
Mrk 573	0.017	123.	N	7.28	44.44	I	SY2
Mrk 622	0.023	100.	N	6.92	44.52	I	SY2
Mrk 686	0.014	144.	N	7.56	44.11	I	SY2
Mrk 917	0.024	149.	N	7.62	44.75	I	SY2
Mrk 1018	0.042	195.	N	8.09	44.39	I	SY2
Mrk 1040	0.017	151.	N	7.64	44.53	I	SY2
Mrk 1066	0.012	105.	N	7.01	44.55	I	SY2
Mrk 1157	0.015	95.	N	6.83	44.27	I	SY2
Akn 79	0.018	143.	N	7.54	45.24	F	SY2
Akn 347	0.023	186.	N	8.00	44.84	F	SY2
IC 5063	0.011	160.	N	7.74	44.53	I	SY2
II ZW55	0.025	212.	N	8.23	44.54	F	SY2
F 341	0.016	114.	N	7.15	44.13	I	SY2
UGC 3995	0.016	155.	N	7.69	44.39	I	SY2
UGC 6100	0.029	156.	N	7.70	44.48	I	SY2
1ES 1959+65	0.048	195.	F	8.09	-		BLL
Mrk 180	0.045	209.	Ba	8.21	-		BLL
Mrk 421	0.031	219.	Ba	8.29	-		BLL
Mrk 501	0.034	372.	Ba	9.21	-		BLL
I Zw 187	0.055	171.	Ba	7.86	-		BLL

Table 5—Continued

Name	z	σ	ref.	M_{BH}	L_{bol}	Type
3C 371	0.051	249.	Ba	8.51	-	BLL
1514-241	0.049	196.	Ba	8.10	-	BLL
0521-365	0.055	269.	Ba	8.65	-	BLL
0548-322	0.069	202.	Ba	8.15	-	BLL
0706+591	0.125	216.	Ba	8.26	-	BLL
2201+044	0.027	197.	Ba	8.10	-	BLL
2344+514	0.044	294.	Ba	8.80	-	BLL
3C 29	0.045	208.	B	8.20	-	RG
3C 31	0.017	248.	B	8.50	-	RG
3C 33	0.059	230.	B	8.38	-	RG
3C 40	0.018	171.	B	7.86	-	RG
3C 62	0.148	273.	B	8.67	-	RG
3C 76.1	0.032	200.	B	8.13	-	RG
3C 78	0.029	261.	B	8.60	-	RG
3C 84	0.017	246.	B	8.49	-	RG
3C 88	0.030	189.	B	8.03	-	RG
3C 89	0.139	250.	B	8.52	-	RG
3C 98	0.031	173.	B	7.88	-	RG
3C 120	0.033	200.	B	8.13	-	RG
3C 192	0.060	192.	B	8.06	-	RG
3C 196.1	0.198	210.	B	8.21	-	RG
3C 223	0.137	202.	B	8.15	-	RG
3C 293	0.045	185.	B	7.99	-	RG
3C 305	0.041	178.	B	7.92	-	RG
3C 338	0.030	290.	B	8.78	-	RG
3C 388	0.091	365.	B	9.18	-	RG
3C 444	0.153	155.	B	7.68	-	RG
3C 449	0.017	224.	B	8.33	-	RG
gin 116	0.033	285.	B	8.75	-	RG
NGC 315	0.017	311.	B	8.90	-	RG
NGC 507	0.017	329.	B	9.00	-	RG

Table 5—Continued

Name	z	σ	ref.	M_{BH}	L_{bol}	Type
NGC 708	0.016	241.	B	8.46	-	RG
NGC 741	0.018	280.	B	8.72	-	RG
NGC 4839	0.023	244.	B	8.48	-	RG
NGC 4869	0.023	199.	B	8.12	-	RG
NGC 4874	0.024	266.	B	8.63	-	RG
NGC 6086	0.032	322.	B	8.96	-	RG
NGC 6137	0.031	295.	B	8.81	-	RG
NGC 7626	0.025	324.	B	8.97	-	RG
0039-095	0.000	280.	B	8.72	-	RG
0053-015	0.038	297.	B	8.82	-	RG
0053-016	0.043	249.	B	8.51	-	RG
0055-016	0.045	302.	B	8.85	-	RG
0110+152	0.044	196.	B	8.09	-	RG
0112-000	0.045	252.	B	8.53	-	RG
0112+084	0.000	365.	B	9.18	-	RG
0147+360	0.018	242.	B	8.46	-	RG
0131-360	0.030	251.	B	8.53	-	RG
0257-398	0.066	219.	B	8.29	-	RG
0306+237	0.000	249.	B	8.51	-	RG
0312-343	0.067	257.	B	8.57	-	RG
0325+024	0.030	219.	B	8.29	-	RG
0431-133	0.033	269.	B	8.65	-	RG
0431-134	0.035	222.	B	8.31	-	RG
0449-175	0.031	158.	B	7.72	-	RG
0546-329	0.037	389.	B	9.29	-	RG
0548-317	0.034	123.	B	7.28	-	RG
0634-206	0.056	195.	B	8.09	-	RG
0718-340	0.029	331.	B	9.01	-	RG
0915-118	0.054	275.	B	8.69	-	RG
0940-304	0.038	389.	B	9.29	-	RG
1043-290	0.060	229.	B	8.37	-	RG

Table 5—Continued

Name	z	σ	ref.	M_{BH}	L_{bol}	Type
1107-372	0.010	295.	B	8.81	-	RG
1123-351	0.032	447.	B	9.53	-	RG
1258-321	0.015	263.	B	8.61	-	RG
1333-337	0.013	288.	B	8.77	-	RG
1400-337	0.014	309.	B	8.89	-	RG
1404-267	0.022	295.	B	8.81	-	RG
1510+076	0.053	336.	B	9.03	-	RG
1514+072	0.035	269.	B	8.65	-	RG
1520+087	0.034	220.	B	8.29	-	RG
1521-300	0.020	166.	B	7.80	-	RG
1602+178	0.041	213.	B	8.24	-	RG
1610+296	0.032	322.	B	8.96	-	RG
2236-176	0.070	245.	B	8.49	-	RG
2322+143	0.045	204.	B	8.17	-	RG
2322-122	0.082	224.	B	8.33	-	RG
2333-327	0.052	269.	B	8.65	-	RG
2335+267	0.030	345.	B	9.08	-	RG

[a]Column (1) name, (2) redshift, (3) stellar velocity dispersion (km s^{-1}), (4) reference for σ, (5) black hole mass estimated using $M_{BH} \propto \sigma^{4.02}$ relation (Equation 4) in units of log $M_{\odot}$. (6) Log of the bolometric luminosity (ergs s^{-1}). For BL Lac objects and radio galaxies, bolometric luminosity is not estimated because of uncertain effects of relativistic beaming and/or nuclear obscuration. (7) Method for bolometric luminosity estimation (I: flux integration; F: SED fitting). (8) AGN type: SY1: Seyfert 1; SY2: Seyfert 2; BLL: BL Lac object; RG: radio galaxy.

References. — N: Nelson (1995); F: Falomo et al. (2002); Ba: Barth et al. (2002); B: Bettoni et al. (2001)

Table 6. Black Hole Masses from Fundamental Plane-Derived Velocity Dispersions

Name	z	$\mu_{1/2}$	r_e(kpc)	ref.	σ(km/s)	M_{BH}	Type
0122+090	0.339	20.64	4.13	1	298.	8.82	BLL
0145+138	0.124	20.91	3.43	1	237.	8.42	BLL
0158+001	0.229	21.88	5.87	1	194.	8.08	BLL
0229+200	0.139	21.07	6.97	1	378.	9.24	BLL
0257+342	0.247	21.28	5.68	1	270.	8.66	BLL
0317+183	0.190	22.56	8.82	1	181.	7.95	BLL
0331-362	0.308	22.09	11.54	1	285.	8.75	BLL
0347-121	0.188	20.63	3.37	1	270.	8.65	BLL
0350-371	0.165	20.77	4.16	1	296.	8.82	BLL
0414+009	0.287	22.78	16.78	1	256.	8.56	BLL
0419+194	0.512	19.71	1.91	1	263.	8.61	BLL
0506-039	0.304	21.21	5.91	1	285.	8.75	BLL
0525+713	0.249	21.10	6.46	1	334.	9.03	BLL
0607+710	0.267	21.76	8.19	1	269.	8.65	BLL
0737+744	0.315	21.41	7.92	1	318.	8.94	BLL
0922+749	0.638	19.79	4.40	1	467.	9.61	BLL
0927+500	0.188	21.55	5.39	1	225.	8.34	BLL
0958+210	0.344	20.13	3.25	1	334.	9.03	BLL
1104+384	0.031	19.50	2.25	1	413.	9.39	BLL
1133+161	0.460	21.75	7.09	1	223.	8.32	BLL
1136+704	0.045	20.05	2.50	1	320.	8.95	BLL
1207+394	0.615	20.73	6.14	1	348.	9.10	BLL
1212+078	0.136	21.35	7.17	1	327.	8.99	BLL
1215+303	0.130	23.31	16.98	1	199.	8.12	BLL
1218+304	0.182	21.64	6.84	1	259.	8.58	BLL
1221+245	0.218	21.39	3.73	1	182.	7.97	BLL
1229+643	0.164	20.42	4.87	1	417.	9.41	BLL
1248-296	0.370	20.57	4.53	1	331.	9.01	BLL
1255+244	0.141	21.36	5.42	1	259.	8.58	BLL
1407+595	0.495	21.01	8.26	1	391.	9.30	BLL
1418+546	0.152	21.51	8.39	1	334.	9.03	BLL

Table 6—Continued

Name	z	$\mu_{1/2}$	r_e(kpc)	ref.	σ(km/s)	M_{BH}	Type
1426+428	0.129	20.62	4.55	1	354.	9.13	BLL
1440+122	0.162	22.21	9.41	1	238.	8.44	BLL
1534+014	0.312	21.47	7.50	1	294.	8.80	BLL
1704+604	0.280	20.30	2.99	1	289.	8.77	BLL
1728+502	0.055	21.08	3.06	1	200.	8.13	BLL
1757+703	0.407	20.51	3.67	1	285.	8.75	BLL
1807+698	0.051	18.60	1.90	1	618.	10.10	BLL
1853+671	0.212	21.37	4.40	1	211.	8.23	BLL
2005-489	0.071	21.30	6.89	1	335.	9.03	BLL
2143+070	0.237	21.68	6.64	1	241.	8.46	BLL
2200+420	0.069	21.80	5.71	1	212.	8.23	BLL
2254+074	0.190	22.48	13.29	1	264.	8.62	BLL
2326+174	0.213	21.13	5.29	1	284.	8.74	BLL
2356-309	0.165	21.08	4.52	1	262.	8.60	BLL
0230-027	0.239	21.80	5.13	2	182.	7.97	RG
0307+169	0.256	21.40	6.27	2	271.	8.66	RG
0345+337	0.244	23.30	8.73	2	112.	7.12	RG
0917+459	0.174	23.00	14.60	2	209.	8.21	RG
0958+291	0.185	22.00	5.67	2	178.	7.93	RG
1215-033	0.184	22.00	5.67	2	179.	7.93	RG
1215+013	0.118	21.00	3.13	2	209.	8.20	RG
1330+022	0.215	22.90	10.47	2	167.	7.82	RG
1342-016	0.167	22.90	15.53	2	234.	8.41	RG
2141+279	0.215	23.50	16.53	2	168.	7.82	RG
0257+024	0.115	21.70	7.80	2	285.	8.75	RQQ
1549+203	0.250	22.20	3.33	2	100.	6.92	RQQ
2215-037	0.241	21.40	4.47	2	208.	8.20	RQQ
2344+184	0.138	23.80	11.67	2	109.	7.07	RQQ

[a]Column (1) name, (2) redshift, (3) surface brightness at r_e in the R band, (4) effective radius scaled with H_0=75 km s^{-1}, (5) reference for original μ_e and r_e (1=Urry et al. 2000, 2=Dunlop et al. 2002), (6) stellar velocity dispersion esimated using μ_e and r_e (Eq. 5). (7) log of black hole mass in solar masses estimated from Eq. 4, with σ derived from μ_e, r_e, and the fundamental plane relation, (8) AGN type (BLL=BL Lac object, RG=radio galaxy, RQQ=radio-quiet quasar).